tal internal reflection fluorescence (TIRF) microscopy (also called evanescent wave microscopy), which allows fluorescence excitation within a closely restricted domain close to the plasma membrane (within 100 nm) [16], has permitted us to observe not only single granule movement underlying exocytosis [17, 18], but also the single molecules on the plasma membrane [19, 20]. Thus, we were able to observe using TIRF microscopy with high resolution, the single insulin granules approaching, docking, and fusing with the plasma membrane, and the spatial localisation of t-SNAREs such as syntaxin-1 and SNAP-25 in the plasma membrane of live cells.

In the present study, a TIRF system was utilised to address the question of whether t-SNAREs are related to the docking and fusion of insulin granules using insulin-treated and/or untreated diabetic Goto–Kakizaki (GK) beta cells where the expression levels of t-SNAREs and docking/fusion of insulin granules were changed. We demonstrate that t-SNAREs are closely associated with the number of docked insulin granules, in parallel with the fusion events from previously docked granules.

Materials and methods

Cells. Diabetic GK rats and non-diabetic male Wistar rats were obtained from a commercial breeder (Oriental Yeast, Tokyo, Japan). The rats were given free access to food and water until the start of experiments, which were conducted with 10-week-old male rats. The body weight of GK rats was not statistically different from that of controls. The plasma glucose concentration in the fed state, measured by the glucose oxidase method, was 12.3±0.78 mmol/l (n=16) in GK rats and 5.8±0.61 mmol/l (n=18) in control rats respectively (p<0.0001). For the normalisation of hyperglycaemia, human insulin (Humalin N; Lilly, Indianapolis, Ala., USA) was injected subcutaneously at 08.00 (2 U/rat) and 20.00 (4 U/rat) hours daily for 2 weeks. Pancreatic islets of Langerhans were isolated by collagenase digestion [10], with some modification. Isolated islets were dissociated into single cells by incubation in Ca^{2+}-free KRB containing 1 mmol/l EGTA, and cultured on fibronectin-coated (KOKEN, Tokyo, Japan) high-refractive-index glass (Olympus, Tokyo, Japan) in RPMI 1640 medium supplemented with 10% FBS (Invitrogen Gibco BRL, Carlsbad, Calif., USA), 200 U/ml penicillin, and 200 µg/ml streptomycin at 37 °C in an atmosphere of 5% CO_2.

Immunohistochemical analysis. Pancreatic beta cells were fixed, made permeable with 2% paraformaldehyde/0.1% Triton X-100, and processed for immunocytochemistry as described previously [9]. Cells were labelled with monoclonal anti-insulin antibodies (Sigma–Aldrich, St. Louis, Mo., USA), anti-HPC1-antibodies (Sigma-Aldrich), and anti-SNAP-25 antibodies (Wako, Osaka, Japan), and then processed with Cy3-conjugated anti-mouse IgG (Amersham Biosciences, Little Chalfont, UK). F-actin was stained by incubation with fluorescein isothiocyanate-conjugated phalloidin (Sigma-Aldrich). For double-immunostaining study, syntaxin-1 was stained with polyclonal anti-HPC-1-antiserum [5] and fluorescein anti-rabbit IgG (Jackson Immuno Research Laboratories, Bar Harbor, Me., USA). Immunofluorescence staining was detected by TIRF or epifluorescence microscopy.

TIRF microscopy. The Olympus total internal reflection system was used with minor modifications as described previously [18]. Light from an Ar laser (488 nm) or an He/Ne laser (543 nm) was introduced to an inverted epifluorescence microscope (IX70, Olympus) through a single-mode fibre and two illumination lenses; the light was focused at the back focal plane of a high-aperture objective lens (Apo 100× OHR; NA 1.65, Olympus). To observe the fluorescence image of Cy3, we

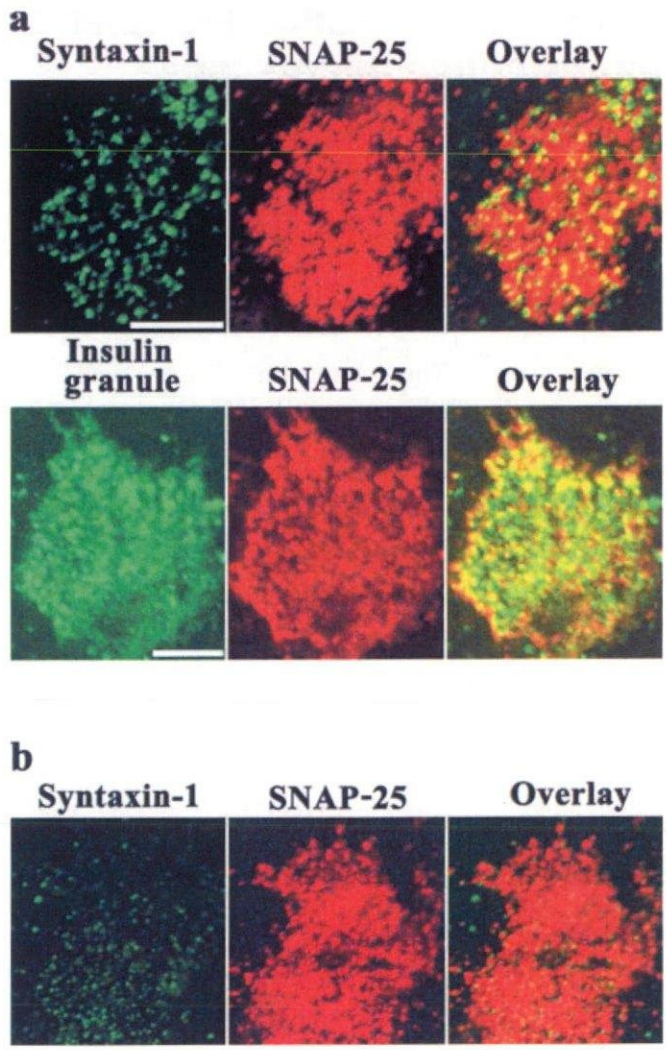

Fig. 1. SNAP-25 colocalised with syntaxin-1 and insulin granules on the plasma membrane of a primary rat pancreatic beta cell. **a.** TIRF images in a normal primary beta cell. After normal rat pancreatic beta cells were prepared, they were fixed, immunostained for syntaxin-1, SNAP-25 or insulin, and viewed simultaneously by TIRF microscopy as described [23]. The colocalisation of syntaxin-1 and SNAP-25, and of SNAP-25 and insulin granules is demonstrated by the superposition (yellow colour) of red and green channel images. **b.** TIRF image of SNAP-25-infected diabetic GK beta cell plasma membrane. Two days after GK beta cells were infected with Adex1CA SNAP-25, they were fixed, immunostained for syntaxin-1 and SNAP-25, and viewed by TIRF microscopy. The overlay of the images shows that most of the syntaxin-1 clusters were overlapped on SNAP-25 clusters

used a 543-nm laser line and a long-pass 590-nm filter. To observe green fluorescent protein (GFP) or fluorescein, we used a 488-nm laser line for excitation and a 515-nm pass filter for the barrier. The procedure for monitoring the GFP-labelled insulin granule motion in primary rat pancreatic beta cells is described elsewhere [21]. Briefly, primary beta cells expressing insulin–GFP on the glass cover slip (Olympus) were mounted in an open chamber and then transferred to the thermostat-controlled stage (37 °C). Cells were stimulated by 22 mmol/l glucose (final), and the measured penetration depths were about 45 nm.

Preparation of recombinant adenoviruses and adenovirus-mediated gene transduction. The construction of expression vectors and recombinant adenovirus encoding insulin–GFP and SNAP-25 has been previously described [10, 21]. To label

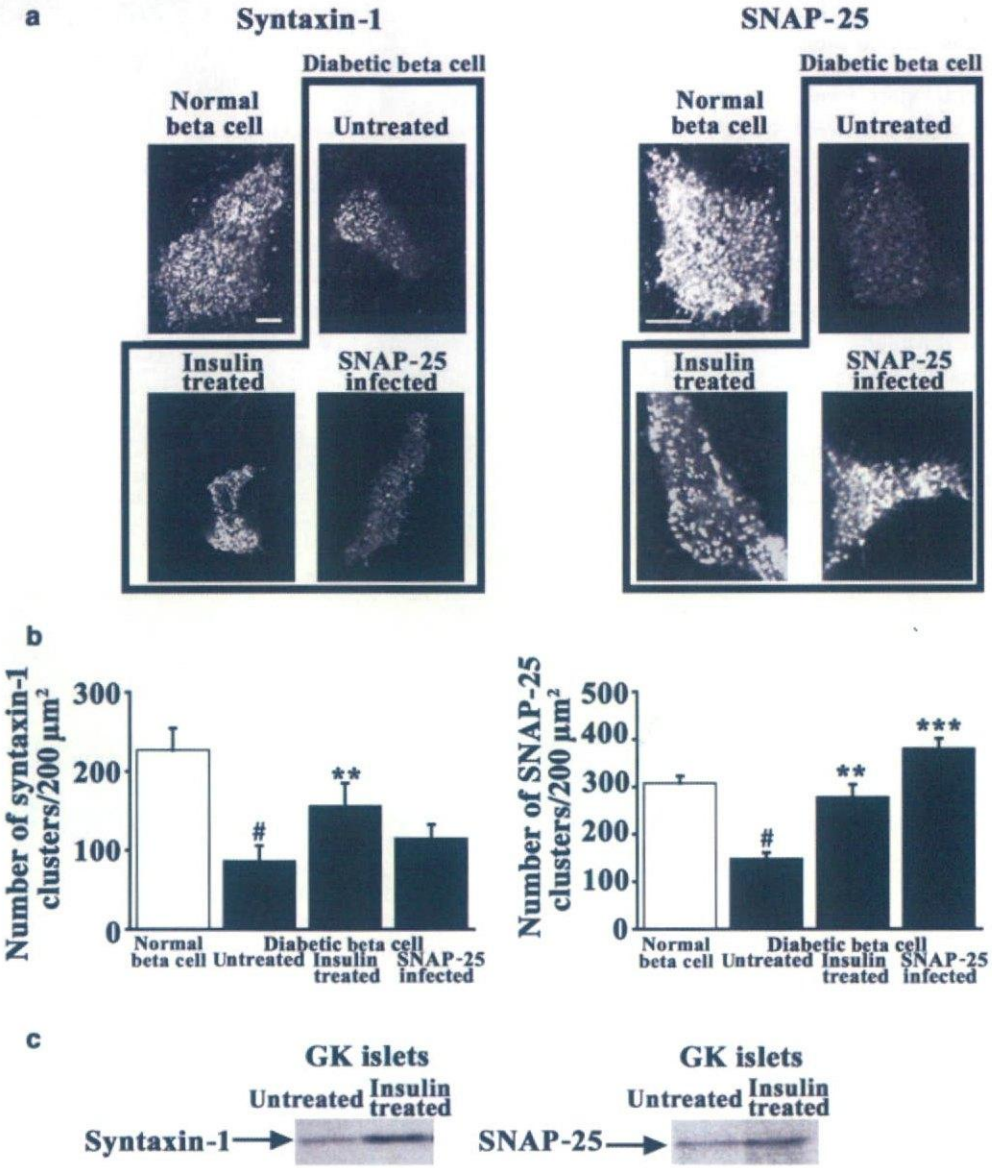

Fig. 2. TIRF images, and the immunoblot analysis of syntaxin-1 and SNAP-25 in normal and diabetic GK beta cells. **a.** Effects of insulin treatment and Adex1CA SNAP-25 infection on syntaxin-1 and SNAP-25 on the plasma membrane of diabetic GK beta cells were shown by TIRF images. Insulin-treated group: GK rats were treated with and/or without a daily subcutaneous injection of human insulin for 2 weeks, and then pancreatic beta cells were prepared. Adex1CA SNAP-25 infected group: the pancreatic beta cells prepared from GK rats were infected with Adex1CA SNAP-25 or Adex 1w (empty virus) and cultured for 2 days as described in Materials and methods. Treated GK or non-treated normal pancreatic beta cells were prepared and fixed, and then immunostained for syntaxin-1 and SNAP-25 before being observed by TIRF microscopy. The scale bars represent 5 μm. Each image is representative of separate experiments. **b.** The number of syntaxin-1 and SNAP-25 clusters in the plasma membrane. Individual fluorescent spots of syntaxin-1 and SNAP-25 shown in TIRF images were counted (normal beta cells, n=10; diabetic beta cells, n=8). The number of clusters was calculated per 200 μm². # $p<0.01$ vs normal, ** $p<0.01$ vs untreated, *** $p<0.001$ vs untreated beta cells. **c.** Immunoblot analysis. Islet proteins (200 islets) were extracted from insulin-treated and -untreated GK rat pancreas, subjected to SDS-PAGE, and immunoblotted with the indicated antibodies, which was followed by chemiluminescence reaction. Each immunoblot is a representation of three separate experiments. The levels of the protein bands were determined using the NIH Image program

the insulin secretory granules, cultured single cells were incubated with RPMI 1640 medium (5% FBS) and the required adenovirus (Adex1CA insulin–GFP, 30 MOI per cell) for 1 h at 37 °C, after which RPMI 1640 medium with 10% FBS was added. For SNAP-25 infection study, cultured single cells were infected with Adex1CA SNAP-25 (20 MOI per cell) prior to labelling the granules with Adex1CA insulin–GFP. Experiments were performed 2 days after the final infection.

Acquiring the images and analysis. Images were collected by a cooled charge-coupled-device camera (Micromax, MMX-512-BFT; Roper Scientific, Princeton Instruments, Trenton, N.J., USA) operated with Metamorph 4.6; Universal Imaging, Downingtown, Pa., USA) as described previously [21]. Most analyses, including counting the number of fluorescent spots, tracking (the single projection of different images) area calculations and fluorescent intensity, were performed using Metamorph software. To analyse the fusion data, fusion events were manually selected, and the average fluorescence intensity of individual granules in a 1-μm×1-μm square placed over the granule centre was calculated. The number of fusion events was manually counted while looping 15,000 frame time-lapses. TIRF images were finally exported as single TIFF files and were further processed using Adobe Photoshop 6.0.

Immunoblotting. Islets prepared from insulin-treated and/or insulin-untreated GK or normal Wistar rats were disrupted by sonication, boiled in SDS sample buffer with 10 mmol/l dithiothreitol, subjected to SDS-PAGE, and then transferred onto nitrocellulose filters. Immunoblotting procedures were performed as described previously [10] using anti-HPC-1-antibodies, anti-SNAP-25 antibodies, and anti-actin monoclonal antibody (Chemicon International, Temecula, Calif., USA). The protein bands were scanned and analysed by NIH Image.

Insulin release from islets. GK islets prepared before and after 2 weeks of daily insulin injection were preincubated with 2.2 mmol/l glucose in KRB for 1 h. They were then challenged with 22 mmol/l glucose plus forskolin (20 μmol/l). The media were collected at the end of the challenge period, then analysed for immunoreactive insulin by radioimmunoassay as previously described [9].

Statistical analysis. Results are means ± SEM, and statistical analysis was performed using ANOVA followed by Fisher's test and regression analysis using the Statview software (Abacus Concepts, Berkeley, Calif., USA).

Results

Decrease in the number of t-SNARE clusters and docked insulin granules in diabetic GK beta cell plasma membrane. A recent study using PC12 cells reported that t-SNAREs are concentrated in separate clusters, shown using membrane–sheet procedures [22]. Consistent with their results, we previously observed, using TIRF microscopy, that t-SNAREs are distributed in numerous spots in the MIN6 cell plasma membrane [23]. In the present study we examined this issue using rat primary pancreatic beta cells. As shown in Fig. 1a, the immunofluorescence of syntaxin-1 and SNAP-25 on the plasma membrane of rat primary pancreatic beta cells was distributed in numerous spots as well as in those observed in MIN6 cells.

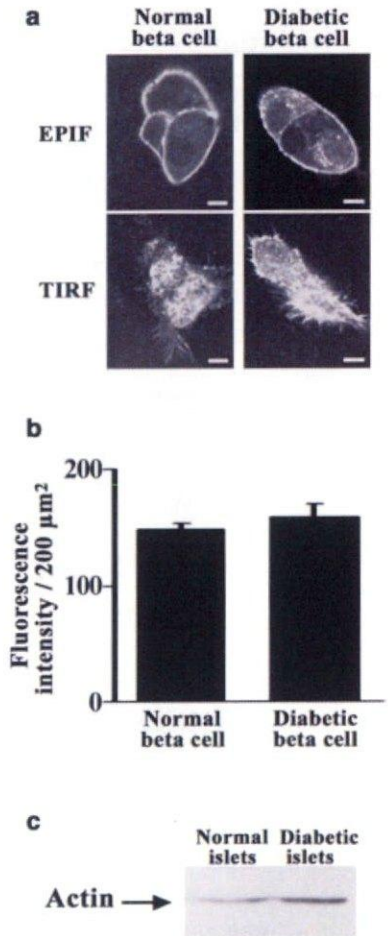

Fig. 3. Immunohistochemistry and immunoblot of actin in normal and diabetic GK beta cells. **a.** TIRF and epifluorescence (EPIF) images of F-actin on the beta cell plasma membrane. After pancreatic beta cells were prepared from normal and GK rat pancreas, F-actin was stained with phalloidin–fluorescein isothiocyanate and observed by TIRF and EPIF microscopy. Each image is representative of three separate experiments. **b.** The fluorescence intensity of phalloidin–fluorescein isothiocyanate analysed by Metamorph based on TIRF image (n=5 cells). **c.** Immunoblot analysis. Islet proteins were subjected to SDS-PAGE, immunoblotted with anti-actin monoclonal antibody, and scanned as described in the legend of Fig. 2 (n=3 for separate experiments)

The apparent diameters of the syntaxin-1 and SNAP-25 clusters were approximately 400 nm, which is similar to that reported in MIN6 cells [23]. Dual-stained immunohistochemical studies for syntaxin-1 and SNAP-25 showed that most of the syntaxin-1 clusters were colocalised with the SNAP-25 clusters, which were also colocalised with insulin granules docked on the plasma membrane (Fig. 1a). Thus, the characterisation of t-SNAREs on the plasma membrane appears not to be different between insulinoma MIN6 cells and primary pancreatic beta cells. We then examined the change of t-SNARE clusters in diabetic GK beta cells. In diabetic GK beta cells, TIRF images and their analyses showed that the number of clusters of syntaxin-1A and SNAP-25 decreased to less than half of that in

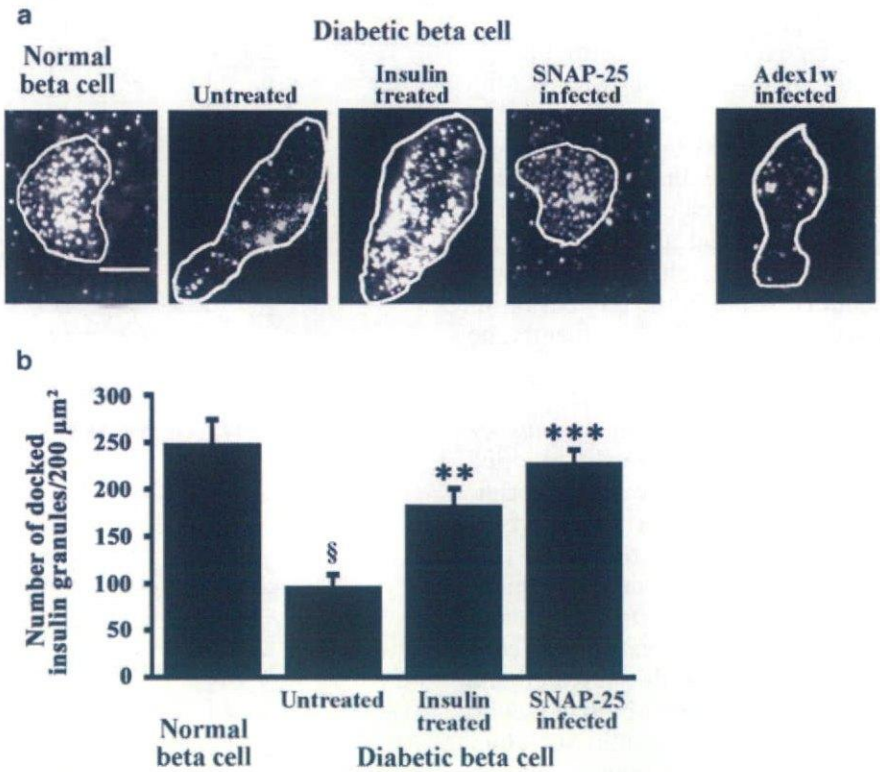

Fig. 4. Histochemical study of insulin secretory granules docked to the plasma membrane. **a.** TIRF images of docked insulin granules in normal and diabetic GK beta cells. For insulin treatment and Adex1CA SNAP-25 or Adex1w infection, GK rats and beta cells were processed as described in the legend of Fig. 2. Cells were fixed with paraformaldehyde, then immunostained for insulin. The surrounding lines represent the outline of cells that are attached to the cover glass. Representative images are shown. The scale bar represents 5 μm. Note that infection with Adex1w empty virus did not affect the docked insulin granules. **b.** The number of insulin granules morphologically docked to the plasma membrane. Individual fluorescent spots shown as TIRF images were counted and calculated per 200 μm² (normal beta cells, n=15; GK beta cells, n=8). § $p<0.0001$ vs normal beta cells, ** $p<0.01$ vs untreated diabetic beta cells, *** $p<0.001$ vs untreated diabetic beta cells

normal beta cells (Fig. 2a, b). To examine whether the decreased number of t-SNARE clusters in diabetic beta cells is a specific phenomenon, we immunostained F-actin as a control. As shown in Fig. 3, no differences in ring-shaped F-actin immunostaining or actin immunoblotting were observed between normal and diabetic beta cells, indicating that the alteration in the number of t-SNARE clusters in the diabetic GK beta cell is a specific phenomenon. Although actin signals in GK islets detected by immunoblot had a tendency to increase, no statistically significant difference was found between normal and GK diabetic islets by scanning and analysis of protein bands with NIH Image (100% vs 148±39%; n=3).

We then examined the change in insulin granules morphologically docked to the plasma membrane in diabetic GK beta cells. There is no precise definition of "morphologically docked granules", but the following are generally used: (i) vesicle is located within 200 nm of the plasma membrane, shown by electron microscopy [24]; (ii) vesicle is located within 100 nm of the surface membrane, shown by electron microscopy [25]; (iii) vesicle distance from plasma membrane is less than 10 nm, shown by TIRF microscopy [26]; and (iv) vesicle is in direct contact with the plasma membrane, shown by electron microscopy [27]. As the penetration depth under our TIRF condition is 80 nm, we defined "morphologically docked granules" as the vesicle being located within 100 nm of the plasma membrane. As shown in Fig. 4a, TIRF imaging depicted the single insulin granules morphologically docked to the plasma membrane, whereby we could manually count the number of docked insulin granules in normal and diabetic beta cells. As shown in Fig. 4b, the number of insulin granules docked to the plasma membrane was markedly reduced in diabetic GK beta cells.

Recovery of the number of t-SNARE clusters and docked insulin granules by insulin treatment. We addressed the question of whether the normalisation of blood glucose levels affects the number of t-SNARE clusters and the number of docked insulin granules in GK beta cells. We treated GK rats with daily insulin injection for 2 weeks, resulting in the reduced blood glucose levels (untreated 11.2±0.61 vs treated 5.6±0.33 mmol/l). After 2 weeks of insulin treatment, pancreatic beta cells were prepared and immunostained with anti-syntaxin-1A, anti-SNAP-25, and anti-insulin antibodies. The number of syntaxin-1 and

SNAP-25 clusters in the plasma membrane was partially, but significantly, recovered to subnormal levels (Fig. 2a, b). Immunoblot analysis also showed that the levels of syntaxin-1A and SNAP-25 were increased in islets isolated from insulin-treated GK rats (Fig. 2c; 182±24% in syntaxin-1, 165±32% in SNAP-25 when expressed as 100% in insulin-untreated GK islets, n=3 for each, p<0.01). It is of note that along with an increase in the number of t-SNARE clusters, there was also an increase of about two-fold in the number of insulin granules docked to the plasma membrane (Fig. 4a, b).

Correlation between the fusion events and the number of docked insulin granules. We previously reported that the fusion events during first-phase release originate from previously docked granules (resident) both in MIN6 cells and primary pancreatic beta cells [18, 21]. In the present study, we tested whether the number of fusion events is correlated with the number of docked insulin granules. After pancreatic beta cells were prepared from normal rats, insulin-untreated and insulin-treated GK rats, they were infected with Adex1CA insulin–GFP to label the insulin secretory granules. After 2 days of infection, granule motion was monitored using TIRF by 22 mmol/l glucose stimulation. In insulin-untreated diabetic GK beta cells, the fusion events from previously docked granules were rarely observed (Fig. 5; untreated). In contrast, in insulin-treated GK beta cells, high glucose stimulation caused fusion events from previously docked insulin granules (Fig. 5; treated) where the number of docked insulin granules was recovered to subnormal levels (see Fig. 4). Furthermore, we measured insulin release from GK islets before and after insulin treatment. Consistent with the results of the TIRF imaging analysis, glucose-stimulated insulin release from insulin-treated GK islets was slightly improved compared with before treatment (1.5±0.3 ng·islet^{-1}·h^{-1} before treatment vs 2.1±0.4 ng islet^{-1}·h^{-1} after treatment, p<0.01, n=3 for separate experiments).

Rescue of fusion events by recovering the number of docked insulin granules and restoring SNAP-25 clusters to normal levels. In order to examine whether the concentration of t-SNARE clusters is linked to the docking status followed by subsequent fusion of insulin granules, we restored the decreased number of SNAP-25 clusters to normal levels by infecting GK beta cells with Adex1CA SNAP-25. GK beta cells infected with Adex1CA SNAP-25 showed the normalised number of SNAP-25 clusters on the plasma membrane (Fig. 2a, b) where the decreased number of docked insulin granules was also restored to subnormal levels (Fig. 4). However, infection with Adex1CA SNAP-25 did not affect the number of syntaxin-1 clusters (Fig. 2a). GK beta cells infected with empty virus Adex 1w did not show any change in the number of SNAP-25 clusters (data not shown) or in the number of docked insulin granules (Fig. 3a). As shown in Fig. 1b, most of the syntaxin-1 clusters were colocalised with SNAP-25 clusters restored by Adex1CA SNAP-25 infection in GK beta cells. Cotransfection of Adex1CA SNAP-25 with Adex1CA syntaxin-1A did not affect the subnormalised number of docked insulin

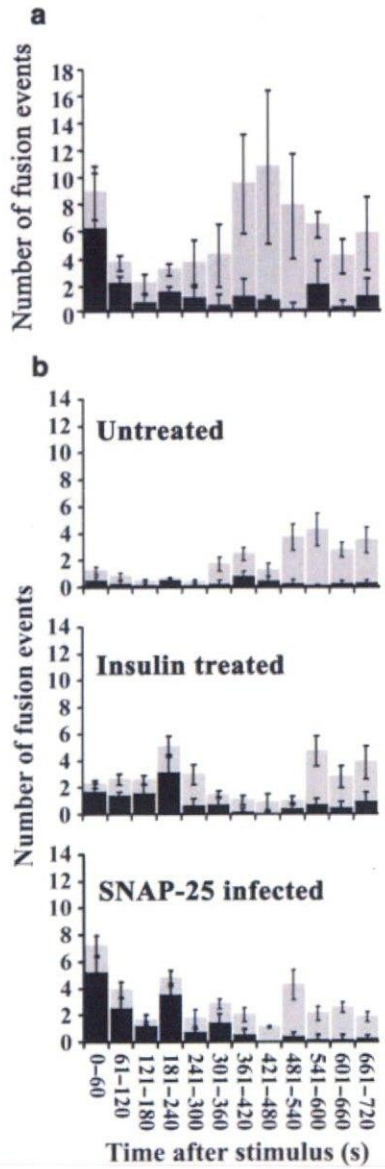

Fig. 5. Restoration of the decreased number of fusion events in normal (**a**) and diabetic (**b**) beta cells. Black bars, resident; grey bars, newcomer. For insulin treatment and SNAP-25 infection, GK beta cells were prepared as in the legend of Fig. 2. After these procedures, beta cells were infected with Adex1CA insulin–GFP in order to label the insulin granules, then the real-time motion of GFP-labelled insulin granules during stimulation with 22 mmol/l glucose was imaged close to the plasma membrane by TIRF, and fusion was analysed by Metamorph software. The graph shows the histogram of the number of fusion events (per 200 μm^2; normal beta cells, n=5; GK beta cells, n=4)

granules (data not shown). We then performed TIRF imaging analysis of the docking and fusion of insulin granules stimulated by 22 mmol/l glucose using Adex1CA-SNAP-25-infected GK beta cells. These beta cells showed a marked increase in fusion events from previously docked granules (Fig. 5; SNAP-25 infected).

Discussion

In the present study, we examined the interaction between the number of t-SNAREs and the number of insulin granules docked to the plasma membrane, and between the number of docked insulin granules and the number of fusion events. Our data demonstrated a close correlation of t-SNARE clusters with docked insulin granules, and that the number of docked insulin granules was correlated with the fusion events from previously docked granules.

TIRF imaging showed that the number of syntaxin-1A and SNAP-25 clusters and the number of docked insulin granules on the plasma membrane decreased in GK beta cells. It is of note that the recovery of the decreased number of SNAP-25 clusters in GK beta cells to normal levels by adenovirus treatment or insulin treatment could restore the number of docked insulin granules, which caused an increased number of fusion events from previously docked granules. We previously reported that restoration of decreased t-SNARE levels improved the impaired insulin secretion in GK islets [10]. At that time, however, we could not know how t-SNARE restoration affects the insulin exocytosis. Now, we know that the restored number of SNAP-25 clusters subnormalised the number of docked insulin granules, through which the fusion from previously docked granules was probably recovered. Thus, in diabetic GK beta cells, the decreased number of t-SNARE clusters may result in impaired insulin granule docking status followed by a decreased fusion event that might lead to the loss of first-phase insulin release. We have recently reported that the disruption of t-SNARE clusters by cholesterol depletion with methyl-β-cyclodextrin treatment causes the inhibition of docking and fusion of insulin granules [23] and thus indicates that impaired formation of t-SNARE clusters in diabetic GK beta cells may be involved in the decreased docking and fusion events of insulin granules.

It is interesting that the transduction with Adex1CA SNAP-25 alone was sufficient to recover the reduced number of docked insulin granules in diabetic GK beta cells, which was followed by an increase in fusion events. Indeed, we had found that the transduction of GK islets with Adex1CA SNAP-25 alone recovered the glucose-stimulated insulin release effectively [10]. Although the precise reason why the restoration of SNAP-25 clusters alone recovered the impaired docking and fusion events in spite of the imbalance in relative levels of SNAP-25 and syntaxin-1 is not known at present, SNAP-25 may be a strict requirement more so than syntaxin-1 in evoked fusion event, as recently shown [28, 29]. Further studies about this important issue are required.

The present study also reported the interesting finding that insulin treatment improved the impaired docking and fusion events in GK beta cells. Although one clinical study showed that the impaired insulin release in diabetic patients was improved when the hyperglycaemia was normalised by daily insulin injection [30], there have been no in vitro studies to examine its mechanism in detail. Judging from our data, it is conceivable that insulin treatment may have reduced the insulin secretion and thus allowed beta cells to increase the number of docked granules. However, because the effects of insulin treatment persisted for at least 2 days during culture period after beta cell preparation, these would be trophic effects. Another simple explanation would be that improved glucotoxicity by insulin treatment may have recovered the beta cell functions.

Finally, we calculated the total number of docked insulin granules in rat pancreatic beta cells. On the basis of our data, we estimated that normal primary beta cells contain approximately 1200 insulin granules docked to the plasma membrane. As the surface area of a beta cell is reported to be 973 μm^2 [31] and the number of docked granules of normal beta cells is calculated to be 246 granules/200 μm^2, the total number of docked insulin granules is about 1200. In a study that used mouse pancreas and electron microscopy [31], Dean reported that the pancreatic beta cells contain about 13,000 insulin granules, and recently, mouse and rat beta cells were reported to have about 10,000 insulin granules per cell, with an estimated number of docked granules of about 600 and 450 respectively [32, 33]. Thus, the number of docked insulin granules is slightly larger in our TIRF imaging analysis. The discrepancy may be because (i) electron microscopy only provides a snapshot of the situation in the beta cells at the time of fixation, so it is not possible to conclude that a certain number of docked granules are really physically attached to the plasma membrane; or (ii) TIRF imaging only gives information on a small part of the cell attached to the coverglass where vesicles are located within 100 nm of the plasma membrane, so the calculated total number of granules docked to the whole cell surface may be an overestimation.

In conclusion, there was an interaction between the number of t-SNARE clusters and the number of docked insulin granules, which were associated with fusion events from previously docked insulin granules.

Acknowledgements. We thank I. Saito for kindly providing the adenovirus cosmid vector and parental virus. This work was supported by Grants-in-Aid for Scientific Research (C)

14570130 (to M. Ohara-Imaizumi) and (B) 15390108 (to S. Nagamatsu) and Scientific Research on Priority Areas 16044240 (to M. Ohara-Imaizumi) from the Japanese Ministry of Education, Culture, Sports, Science and Technology, and by a grant from the Japan Private School Promotion Foundation (to S. Nagamatsu).

References

1. Rothman JE (1994) Mechanisms of intracellular protein transport. Nature 372:55–63
2. Sudhof TC (1995) The synaptic vesicle cycle: a cascade of protein-protein interactions. Nature 375:645–653
3. Jacobsson G, Bean AJ, Scheller RH et al. (1994) Identification of synaptic proteins and their isoform mRNAs in compartments of pancreatic endocrine cells. Proc Natl Acad Sci USA 91:12487–12491
4. Wheeler MB, Sheu L, Ghai M et al. (1996) Characterization of SNARE protein expression in β cell lines and pancreatic islets. Endocrinology 137:1340–1348
5. Nagamatsu S, Fujiwara T, Nakamichi Y et al. (1996) Expression and functional role of syntaxin 1/HPC-1 in pancreatic β cells. J Biol Chem 271:1160–1165
6. Sadoul K, Lang J, Montecucco C et al. (1995) SNAP-25 is expressed in islets of Langerhans and is involved in insulin release. J Cell Biol 128:1019–1028
7. Martin F, Moya F, Gutierrez LM, Reig JA, Soria B (1995) Role of syntaxin in mouse pancreatic beta cells. Diabetologia 38:860–863
8. Kiraly-Borri CE, Morgan A, Burgoyne RD, Weller U, Wollheim CB, Lang J (1996) Soluble N-ethymaleimide-sensitive-factor attachment protein and N-ethylmaleimide-insensitive factors are required for Ca^{2+}-stimulated exocytosis of insulin. Biochem J 314:199–203
9. Nagamatsu S, Watanabe T, Nakamichi Y, Yamamura C, Tsuzuki K, Matsushima S (1999) α-Soluble N-ethylmaleimide-sensitive factor attachment protein is expressed in pancreatic β cells and functions in insulin but not γ-aminobutyric acid secretion. J Biol Chem 274:8053–8060
10. Nagamatsu S, Nakamichi Y, Yamamura C et al. (1999) Decreased expression of t-SNARE, syntaxin 1, and SNAP-25 in pancreatic beta-cells is involved in impaired insulin secretion from diabetic GK rat islets: restoration of decreased t-SNARE proteins improves impaired insulin secretion. Diabetes 48:2367–2373
11. Gaisano HY, Ostenson CG, Sheu L, Wheeler MB, Efendic S (2002) Abnormal expression of pancreatic islet exocytotic soluble N-ethylmaleimide-sensitive factor attachment protein receptors in Goto-Kakizaki rats is partially restored by phlorizin treatment and accentuated by high glucose treatment. Endocrinology 143:4218–4226
12. Zhang W, Khan A, Ostenson CG, Berggren PO, Efendic S, Meister B (2002) Down-regulated expression of exocytotic proteins in pancreatic islets of diabetic GK rats. Biochem Biophys Res Commun 291:1038–1044
13. Lang T, Wacker I, Steyer J et al. (1997) Ca^{2+}-triggered peptide secretion in single cells imaged with green fluorescent protein and evanescent wave microscopy. Neuron 18:857–863
14. Rohrbach A (2000) Observing secretory granules with a multiangle evanescent wave microscopy. Biophys J 78: 2641–2654
15. Johns LM, Levitan ES, Shelden EA, Holz RW, Axelrod DJ (2001) Restriction of secretory granule motion near the plasma membrane of chromaffin cells. J Cell Biol 183: 177–190
16. Axelrod D (2001) Total internal reflection fluorescent microscopy in cell biology. Traffic 2:764–774
17. Schmoranzer J, Goulain M, Axelrod D, Simon SM (2000) Imaging constitutive exocytosis with total internal reflection fluorescence microscopy. J Cell Biol 149:23–31
18. Ohara-Imaizumi M, Nakamichi Y, Tanaka T, Ishida H, Nagamatsu S (2002) Imaging exocytosis of single insulin secretory granules with evanescent wave microscopy. J Biol Chem 277:3805–3808
19. Tokunaga M, Kitamura K, Saito K, Iwane AH, Yanagida T (1997) Single molecule imaging of fluorophores and enzymatic reactions achieved by objective-type total internal reflection fluorescence microscopy. Biochem Biophys Res Commun 235:47–53
20. Sako Y, Uyemura T (2002) Total internal reflection fluorescence microscopy for single-molecule imaging in living cells. Cell Struct Funct 27:357–365
21. Ohara-Imaizumi M, Nishiwaki C, Kikuta T, Nagai S, Nakamichi Y, Nagamatsu S (2004) TIRF imaging of docking and fusion of single insulin granule motion in primary pancreatic β-cells: different behaviour of granule motion between normal and Goto-Kakizaki diabetic rat β-cells. Biochem J 381:13–18
22. Lang T, Bruns D, Wenzel D et al. (2001) SNAREs are concentrated in cholesterol-dependent clusters that define docking and fusion sites for exocytosis. EMBO J 20: 2202–2213
23. Ohara-Imaizumi M, Nishiwaki C, Kikuta T, Kumakura K, Nakamichi Y, Nagamatsu S (2004) Site of docking and fusion of insulin secretory granules in live MIN6 cells analyzed by TAT-conjugated anti-syntaxin 1 antibody and total internal reflection fluorescence microscopy. J Biol Chem 279:8403–8408
24. Ashery U, Varoqueaux F, Voets T et al. (2000) Munc 13-1 acts as a priming factor for large dense-core vesicles in bovine chromaffin cells. EMBO J 19:3586–3596
25. Rizzoli SO, Betz WI (2004) The structural organization of the readily releasable pool of synaptic vesicles. Science 303:2037–2039
26. Zenisek D, Steyer JA, Almers W (2000) Transport, capture and exocytosis of single synaptic vesicles at active zones. Nature 406:849–854
27. Olofsson CS, Gopel SO, Barg S et al. (2002) Fast insulin secretion reflects exocytosis of docked granules in mouse pancreatic β-cells. Eur J Physiol 444:43–51
28. Washbourne P, Thompson PM, Carta M et al. (2002) Genetic ablation of the t-SNARE SNAP-25 distinguishes mechanisms of neuroexocytosis. Nat Neurosci 5:19–26
29. Sorensen JB, Nagy G, Varoqueaux F et al. (2003) Differential control of the releasable vesicle pools by SNAP-25 splice variants and SNAP-23. Cell 114:75–86
30. Garvey WT, Olefsky JM, Griffin J, Hamman RF, Kolterman OG (1985) The effect of insulin treatment on insulin secretion and insulin action in type II diabetes mellitus. Diabetes 34:222–234
31. Dean PM (1973) Ultrastructural morphometry of the pancreatic β-cell. Diabetologia 9:115–119
32. Rorsman P, Renstrom E (2003) Insulin granule dynamics in pancreatic beta cells. Diabetologia 46:1029–1045
33. Braun M, Wendt A, Birnir B et al. (2004) Regulated exocytosis of GABA-containing synaptic-like microvesicles in pancreatic β-cells. J Gen Physiol 123:191–204

Rab27a mediates the tight docking of insulin granules onto the plasma membrane during glucose stimulation

Kazuo Kasai,[1] Mica Ohara-Imaizumi,[2] Noriko Takahashi,[3,4] Shin Mizutani,[1] Shengli Zhao,[1] Toshiteru Kikuta,[2] Haruo Kasai,[3] Shinya Nagamatsu,[2] Hiroshi Gomi,[1] and Tetsuro Izumi[1]

[1]Department of Molecular Medicine, Institute for Molecular and Cellular Regulation, Gunma University, Maebashi, Japan. [2]Department of Biochemistry, Kyorin University School of Medicine, Mitaka, Japan. [3]Department of Cell Physiology, National Institute for Physiological Sciences and the Graduate University of Advances Studies, Okazaki, Japan. [4]Precursory Research for Embryonic Science and Technology, Japan Science and Technology Agency, Kawaguchi, Japan.

The monomeric small GTPase Rab27a is specifically localized on both secretory granules and lysosome-related organelles. Although natural mutations of the Rab27a gene in human Griscelli syndrome and in *ashen* mice cause partial albinism and immunodeficiency reflecting the dysfunction of lysosome-related organelles, phenotypes resulting from the defective exocytosis of secretory granules have not been reported. To explore the roles of Rab27a in secretory granules, we analyzed insulin secretion profiles in *ashen* mice. *Ashen* mice showed glucose intolerance after a glucose load without signs of insulin resistance in peripheral tissues or insulin deficiency in the pancreas. Insulin secretion from isolated islets was decreased specifically in response to high glucose concentrations but not other nonphysiological secretagogues such as high K^+ concentrations, forskolin, or phorbol ester. Neither the intracellular Ca^{2+} concentration nor the dynamics of fusion pore opening after glucose stimulation were altered. There were, however, marked reductions in the exocytosis from insulin granules predocked on the plasma membrane and in the replenishment of docked granules during glucose stimulation. These results provide the first genetic evidence to our knowledge for the role of Rab27a in the exocytosis of secretory granules and suggest that the Rab27a/effector system mediates glucose-specific signals for the exocytosis of insulin granules in pancreatic β cells.

Introduction

Membrane traffic is fundamental to the integrity of eukaryotic cells and is regulated by conserved protein families, such as soluble *N*-ethylmaleimide–sensitive factor attachment protein receptors (SNAREs) and Rab GTPases. Compared with the established roles of SNARE proteins, which mediate membrane fusion through the formation of a 4-helix bundle in a protein complex, the functions of Rab proteins often remain elusive. This may be because Rab proteins appear to play modulatory roles rather than mechanical ones and because they execute versatile functions by binding to various types of effector proteins. Furthermore, the potentially redundant functions of numerous Rab proteins differentiated in higher eukaryotes might obscure the phenotypes of individual mutants in genetic studies.

Among Rabs, the Rab27 subfamily, which consists of Rab27a and Rab27b, is known to function in regulated secretory pathways (1, 2). Each of these pathways harbors a specific organelle that stores bioactive substances and releases them in response to extracellular stimuli. Two major types of organelles can be distinguished by their morphological appearance, release kinetics, and biogenesis: synaptic vesicles in neurons and secretory granules in endocrine and exocrine cells (3). Recently, a third class of organelles, those that are released in a regulated fashion, has been identified; these are called lysosome-related organelles or secretory lysosomes (4). These organelles, which include melanosomes in melanocytes and lytic granules in cytotoxic T-lymphocytes, have unique biogenesis related to lysosomes and distinct modes of exocytosis. Rab27a and/or Rab27b are commonly located on these secretory organelles and regulate the exocytosis using multiple effector proteins (5, 6). Importantly, mutations of the Rab27a gene discovered in human Griscelli syndrome (7) and in the mouse coat-color mutant *ashen* (8) cause partial albinism and immunodeficiency, reflecting the dysfunction of lysosome-related organelles. By contrast, phenotypes that result from defects in the exocytosis of secretory granules have not been reported either in these human subjects or in mice, although Rab27a is clearly demonstrated to be localized on secretory granules and to affect hormone secretion in endocrine cells (9).

In the present study, we examined the exocytosis of insulin granules of Rab27a-mutated *ashen* mice, because the functional roles of Rab27a and its effector granuphilin have been most extensively studied among secretory granules (9–12). By using various morphological, physiological, and biochemical techniques, we found that insulin secretion is impaired specifically in response to a physiological secretagogue, glucose, but not to other, nonphysiological secretagogues. The exocytosis from insulin granules predocked on the plasma membrane and the refilling of docked granules during glucose stimulation were markedly affected in pancreatic β cells of *ashen* mice. This study is the first to our knowledge to provide in vivo genetic evidence for the role of Rab27a in the exocytotic pathway of secretory granules.

Results

Expression of Rab27a, Rab27b, and granuphilin in pancreas. We first examined the expression of Rab27a and its related molecules in pancreatic islets (Figure 1A). As described previously (9), Rab27a

Nonstandard abbreviations used: $[Ca^{2+}]_i$, intracellular Ca^{2+} concentration; K_{ATP} channel, ATP-sensitive K^+ channel; PMA, phorbol-12-myristate-13-acetate; SNARE, soluble *N*-ethylmaleimide–sensitive factor attachment protein receptor; TIRFM, total internal reflection fluorescence microscopy.

Conflict of interest: The authors have declared that no conflict of interest exists.

Citation for this article: *J. Clin. Invest.* **115**:388–396 (2005). doi:10.1172/JCI200522955.

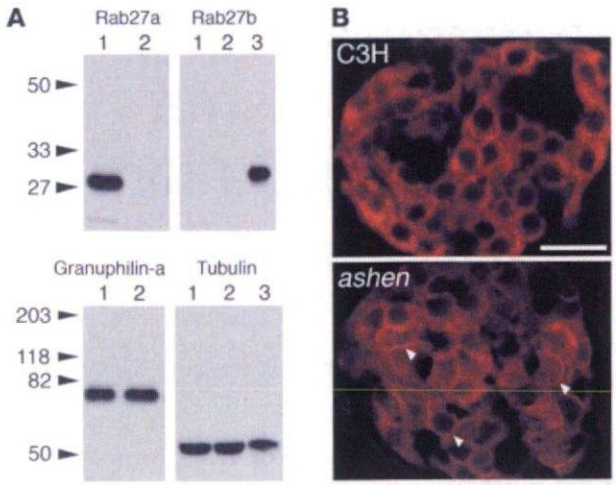

Figure 1
Expression of Rab27a, Rab27b, and granuphilin in pancreatic islets. (**A**) An equal amount of protein (20 μg) from the pancreatic islets of 17-week-old male C3H/He (lane 1) and *ashen* mice (lane 2) was separated by electrophoresis for immunoblotting with anti-Rab27a, anti-Rab27b, or anti-granuphilin (αGrp-aC) antibodies. The expression levels of α-tubulin were also examined for normalization. For the immunoblotting with anti-Rab27b and anti–α-tubulin antibodies, 20 μg of protein from the pituitary of C3H/He mice were loaded on lane 3 for the reference. Numbers to the left of each panel are molecular masses in kDa. (**B**) The pancreas organs of 17-week-old male C3H/He (upper) or *ashen* mice (lower) were immunostained with anti-granuphilin antibodies (αGrp-N). Granuphilin is distinguishably concentrated along the plasma membrane in *ashen* β cells (arrowheads) compared with control β cells, although the expression levels are similar. Scale bar: 20 μm.

protein was highly expressed in pancreatic islets of control C3H/He mice. By contrast, it was not detected in the islets of *ashen* mice, which is consistent with previous reports showing the lack of detectable Rab27a protein in *ashen*-derived cytotoxic T lymphocytes (13, 14) and platelets (15). Because the Rab27a protein is truncated due to a splice site mutation in *ashen* mice (8), the mutant protein either is unstable or loses its immunoreactivity. In either case, the mutant Rab27a protein is probably nonfunctional because it lacks some of the GTP-binding pockets. Rab27b, on the other hand, was barely detectable in the islets but was significantly expressed in the pituitary of control mice, as reported previously (16). The expression level of granuphilin, a Rab27a effector in pancreatic β cells (9), was not altered in *ashen* islets, in contrast to another Rab27a effector, melanophilin, which is severely downregulated in *ashen* melanocytes (17).

Immunohistochemical analysis of mouse pancreas specimens confirmed that Rab27a was expressed in insulin-positive β cells of control C3H/He mice, as reported previously (9), but not in those of *ashen* mice (data not shown). By contrast, Rab27b was expressed in exocrine and peripheral islet cells, but not in β cells (H. Gomi, S. Zhao, and T. Izumi, unpublished observations). The islet architecture of *ashen* mice was normal, including a mantle structure between β and non-β cells, and the expression levels of pancreatic hormones were not significantly reduced in *ashen* islets (data not shown, but see Figure 1B). While the lack of Rab27a did not affect the expression level of its effector granuphilin (Figure 1A), its intracellular location was significantly affected. The distribution of granuphilin was distinguishably shifted to the plasma membrane in *ashen* β cells compared with its diffuse cytoplasmic distribution in control β cells (Figure 1B). Alteration in the subcellular localization in Rab27a-deficient β cells strongly supports our previous proposals that granuphilin is associated with secretory granules through Rab27a and that it is an effector of Rab27a, but not of Rab3a, in vivo, despite its affinities to both Rab proteins in vitro (9).

Glucose tolerance and related in vivo phenotypes. Because Rab27b is coexpressed and functionally redundant with Rab27a in platelets (15), the lack of Rab27b in the pancreatic β cells of *ashen* mice makes them an excellent subject of study for the evaluation of Rab27a function. We first examined in vivo phenotypes that might be affected by potential insulin secretion defects in *ashen* β cells. Body weight (Figure 2A) and blood glucose levels examined in mice fed ad libitum (data not shown) or in fasting mice (Figure 2B) did not differ between *ashen* and C3H/He mice. Blood glucose levels after a glucose load, however, were significantly higher in *ashen* mice (Figure 2B). Although it is generally difficult to measure small changes in plasma insulin levels accurately from a limited amount of samples in mice, unless they have marked hyperinsulinemia (see the examples in ref. 18), plasma insulin levels at fasting or during a glucose tolerance test were not significantly different, except at 120 minutes after the glucose load, at which point the levels were slightly higher in *ashen* mice (data not shown). Although the hyperglycemia with normoinsulinemia

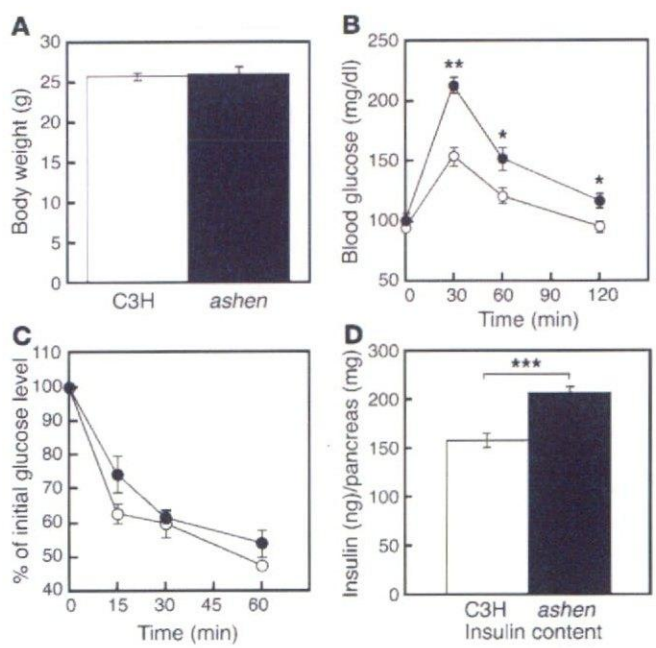

Figure 2
In vivo phenotypes of *ashen* and C3H/He mice. All the phenotypes were derived from male C3H/He (white bars or open circles) or *ashen* (black bars or filled circles) mice. Body weight (**A**), blood glucose concentrations during an intraperitoneal glucose tolerance test (**B**), and total insulin content in the pancreas (**D**) were measured at 15 weeks of age. An intraperitoneal insulin tolerance test (**C**) was performed at 16 weeks of age, and its results are expressed as a percentage of the initial blood glucose concentration. Values are mean ± SE (**A** and **B**, $n = 8$ for C3H/He, $n = 7$ for *ashen*; **C**, $n = 5$ for C3H/He and *ashen*; **D**, $n = 8$ for C3H/He and *ashen*). The statistical significance of differences between means was assessed by Student's t test. $^{*}P < 0.05$, $^{**}P < 0.005$, $^{***}P < 0.0005$ vs. C3H/He mice.

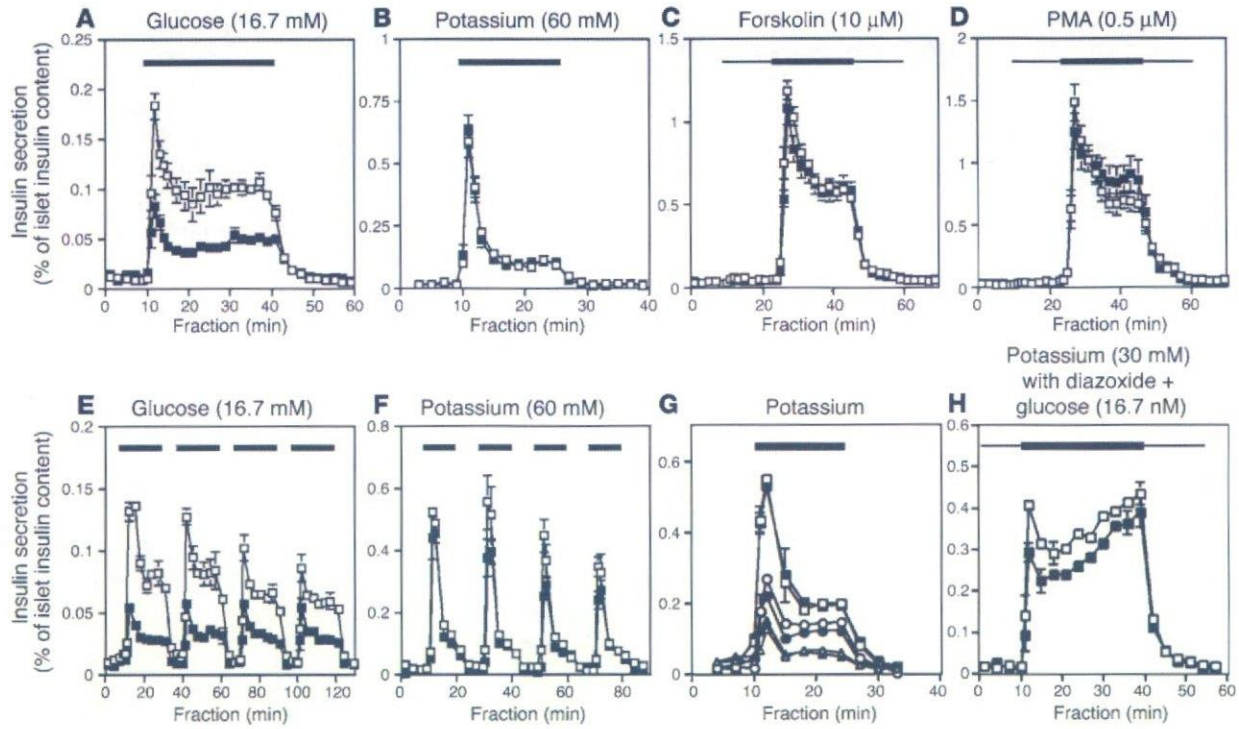

Figure 3

Insulin secretion profiles of perifused islets. Insulin secretion was examined in islets isolated from age-matched (15–17 weeks of age) male C3H/He (open symbols) or *ashen* mice (filled symbols). The islets were stabilized by perifusion of standard low-glucose (2.8 mM) Krebs-Ringer buffer for 10 minutes, after which an appropriate secretagogue was applied. (**A** and **B**) Islets were stimulated by 16.7 mM glucose for 30 minutes (**A**; $n = 9$ for each strain) or with 60 mM KCl for 15 minutes (**B**; $n = 6$). (**C** and **D**) Islets were stimulated by 16.7 mM glucose for 30 minutes in the continuous presence of either forskolin (**C**, 10 mM; $n = 8$) or PMA (**D**, 0.5 mM; $n = 8$). (**E** and **F**) Islets were stimulated 4 times by either 16.7 mM glucose for 20 minutes (**E**; $n = 3$) or by 60 mM KCl for 10 minutes (**F**; $n = 3$), with 10-minute intervals of the standard buffer. (**G**) Islets were stimulated by 60 mM (squares), 30 mM (circles), or 20 mM KCl (triangles) for 15 minutes, followed by the standard buffer for 15 minutes ($n = 3$ for each condition and strain). (**H**) Islets were perifused with buffer containing 250 μM diazoxide and 16.7 mM glucose for 10 minutes. They were further perifused with the buffer containing 30 mM KCl for 30 minutes, in the continuous presence of diazoxide and glucose ($n = 3$ for each strain). Values are mean ± SE.

or slight hyperinsulinemia upon glucose challenge might suggest the presence of insulin resistance, insulin tolerance tests (0.75 U human insulin/kg body weight) revealed comparable insulin sensitivity between *ashen* and control mice (Figure 2C). The tests with smaller doses of insulin (0.1–0.5 U/kg) after overnight fasting also showed similar insulin sensitivity (data not shown). Insulin content in total pancreas was increased by 1.3-fold in *ashen* mice compared with controls (Figure 2D), which may reflect an impairment of insulin secretion. These findings indicate that *ashen* mice have glucose intolerance without signs of insulin resistance in peripheral tissues or absolute insulin deficiency in pancreatic β cells.

Insulin secretion profiles in perifused islets. Because the overexpression of active forms of Rab27a has been shown to augment insulin secretion in the cultured β-cell line MIN6 (9), the lack of functional Rab27a may induce insulin secretion defects in *ashen* mice. We incubated pancreatic islets, isolated from C3H/He or *ashen* mice, overnight in culture medium to decrease potential environmental effects, such as differences in blood glucose levels, in vivo. They were then examined for the ability to secrete insulin in response to several secretagogues by perifusion analyses. Insulin secretion in response to a high glucose level (16.7 mM) was significantly reduced in both the first (approximately 5 minutes) and second phases in *ashen* islets (repeated measure ANOVA, $P < 0.0001$), and the accumulated glucose-induced insulin secretion over 30 minutes was diminished by approximately 50% compared with the control islets (Figure 3A). Surprisingly, the reduction in insulin release was specific to glucose stimulation. Insulin secretion in response to depolarization induced by high K^+ concentration (60 mM) was normal in *ashen* islets (Figure 3B). Furthermore, both forskolin (activator of adenylate cyclase) and phorbol-12-myristate-13-acetate (PMA; protein kinase C activator) stimulated insulin secretion in the presence of high glucose levels indistinguishably between *ashen* and control islets (Figure 3, C and D). These findings indicate that the defect in insulin secretion in *ashen* islets does not simply reflect a general decrease in the releasable pool of granules. Consistent with this idea, insulin secretion was normal even after repeated exposure to high concentrations of K^+ in *ashen* islets (Figure 3F). By contrast, insulin secretion was decreased at each of the repeated exposures to the glucose stimuli (Figure 3E; $P < 0.0001$), suggesting that Rab27a is specifically required for the replenishment of a pool of granules released by glucose.

The stimulation with high K^+, forskolin, or PMA induced much higher insulin secretion compared with the 16.7 mM glucose stimulation (note differences in the ordinates of each panel in Figure 3). Stronger stimuli might have obscured subtle functional differences between the 2 kinds of islets. The lower concentrations of KCl (20 mM or 30 mM) induced an insulin secretion at the

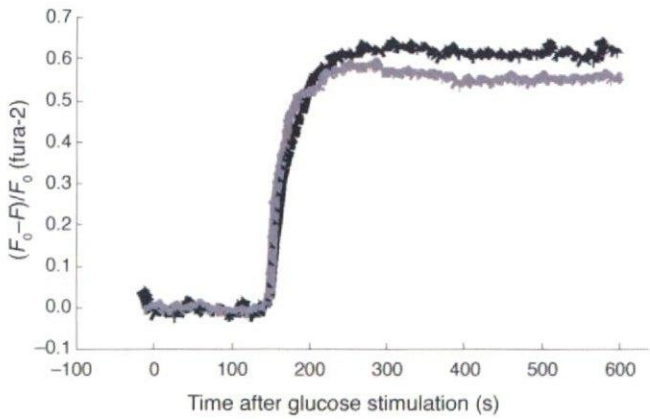

Figure 4
The rise in cytosolic Ca^{2+} concentration in response to glucose stimulation. The cytosolic Ca^{2+} concentration was measured using Fura-2 acetoxymethyl ester by two-photon excitation imaging in pancreatic β cells of either C3H/He (gray) or *ashen* (black) mice and was represented by $(F_0–F)/F_0$, where F_0 and F stand for resting and fluorescence and fluorescence after 20 mM glucose stimulation, respectively. Mean values are shown (n = 4).

peak that was equivalent to that induced by 16.7 mM glucose during perifusion of the control islets (Figure 3, A and G). The same treatment in *ashen* islets evoked an indistinguishable amount and manner of insulin secretion (Figure 3G). Therefore, *ashen* β cells showed specific defects in insulin secretion in response to glucose, but not to high K^+, independent of the strength of the depolarization stimuli. These findings indicate qualitative differences in the mode of exocytosis induced by glucose and that induced by other, nonphysiological secretagogues.

Although high K^+ stimulation physically induces membrane depolarization and a subsequent rise of intracellular Ca^{2+} concentration ($[Ca^{2+}]_i$), glucose stimulates intracellular metabolism and ATP production, which is thought to induce additional effects as well as triggering depolarization by the closure of ATP-sensitive K^+ (K_{ATP}) channel. This amplifying effect by glucose has classically been evaluated by the amount of insulin secreted in the presence of diazoxide, an opener of K_{ATP} channels (19, 20). As expected, 250 μM diazoxide inhibited insulin secretion induced by 16.7 mM glucose in both *ashen* and control islets (see the insulin secretion during the first 10 minutes in Figure 3H). To induce insulin secretion, the islets were depolarized by 30 mM KCl in the continuous presence of diazoxide and 16.7 mM glucose. The amount of insulin secreted was not significantly different, though slightly reduced, in the *ashen* islets compared with the control islets (Figure 3H). These findings suggest that the amplifying pathway by glucose is largely intact in *ashen* β cells.

Analysis of the exocytosis of insulin granules by two-photon excitation imaging. To explore the mechanism responsible for the decrease in glucose-induced insulin secretion, we directly examined the exocytosis of granules by 2-photon excitation imaging (21). This newly innovated morphological technique enables us to precisely monitor individual exocytotic events per the constant area, as well as other parameters relevant to exocytosis, in isolated islets. Both the amplitude and time course of the glucose-induced rise in Ca^{2+} concentration measured using Fura-2 was not different between *ashen* and C3H/He mice (Figure 4 and Table 1), which suggests normal glucose metabolism and ATP production in *ashen* β cells. Fusion pore dynamics examined by measuring latency for the onset of staining with fluorescent markers of different sizes was also unchanged in *ashen* islets (Table 1). However, the exocytotic events during the first and second 5 minutes were significantly reduced (Table 1), which is consistent with the findings of the perifusion assays (Figure 3A). These results independently demonstrated the reduction of glucose-induced fusion events and excluded the possibility of changes in the dynamics of $[Ca^{2+}]_i$ or fusion pore opening in *ashen* islets.

Analysis of the exocytosis of insulin granules by total internal reflection fluorescence microscopy. We next utilized total internal reflection fluorescence microscopy (TIRFM) to investigate the exocytotic events occurring just beneath the plasma membrane in isolated pancreatic β cells. TIRFM detects cytoplasmic events within 100 nm of the plasma membrane (22). We first immunostained endogenous insulin in fixed pancreatic β cells. Because fluorescent imaging by TIRFM can depict the single insulin granules closely associated with the plasma membrane (23), we counted the number of morphologically docked granules (Figure 5A). The *ashen* β cells showed a marked decline in the number (130 ± 34 per 200 μm^2 in *ashen* β cells vs. 219 ± 34 per 200 μm^2 in C3H/He β cells; n = 24 for *ashen* and n = 21 for C3H/He) to 59% of normal levels ($P < 0.0001$). These findings suggest that granules docked onto the plasma membrane are reduced in *ashen* β cells.

We then observed fusion events of fluorescence-labeled granules by TIRFM in live β cells that had been infected with an adenovirus encoding GFP-tagged insulin (23). The fusion events in response to 30 mM KCl occurred predominantly during the first 5 minutes after the stimulation and were not significantly different between *ashen* and control β cells (40.1 ± 5.9 in 0–5 minutes in *ashen* β cells vs. 56.7 ± 6.9 in 0–5 minutes for C3H/H3 β cells, n = 4 each). There were no significant differences in the exocytosis of previously docked granules (4.5 ± 2.1 in *ashen* β cells vs. 7.5 ± 2.0 in C3H/He β cells) or in that of newly recruited granules (34.4 ± 4.4 in *ashen* β cells vs. 47.7 ± 6.9 in C3H/He β cells). The

Table 1
Analysis of the exocytosis of insulin granules by 2-photon excitation imaging

	C3H	*ashen*
Increase in the cytosolic Ca^{2+} concentration in response to 12 mM glucose		
$(F_0–F)/F_0$	0.60 ± 0.03 (n = 10)	0.63 ± 0.02[A] (n = 15)
Exocytotic events within an arbitrary area (2,000 μm^2) in response to 20 mM glucose		
First phase (0–300 seconds)	48.3 ± 8.0	28.8 ± 7.3[B]
Second phase (300–600 seconds)	48.6 ± 10.8 (n = 5)	39.8 ± 6.1[C] (n = 5)
Latency (s) for the onset of staining with sulforhodamine B (about 1.4 nm) relative to that of staining with 10-kDa dextran (about 6 nm)		
	1.6 ± 0.18 (n = 25)	2.0 ± 0.21[A] (n = 31)

The statistical significance of differences between means was assesed by Student's t test. [A]NS ($P > 0.05$). [B]$P < 0.005$. [C]$P < 0.025$.

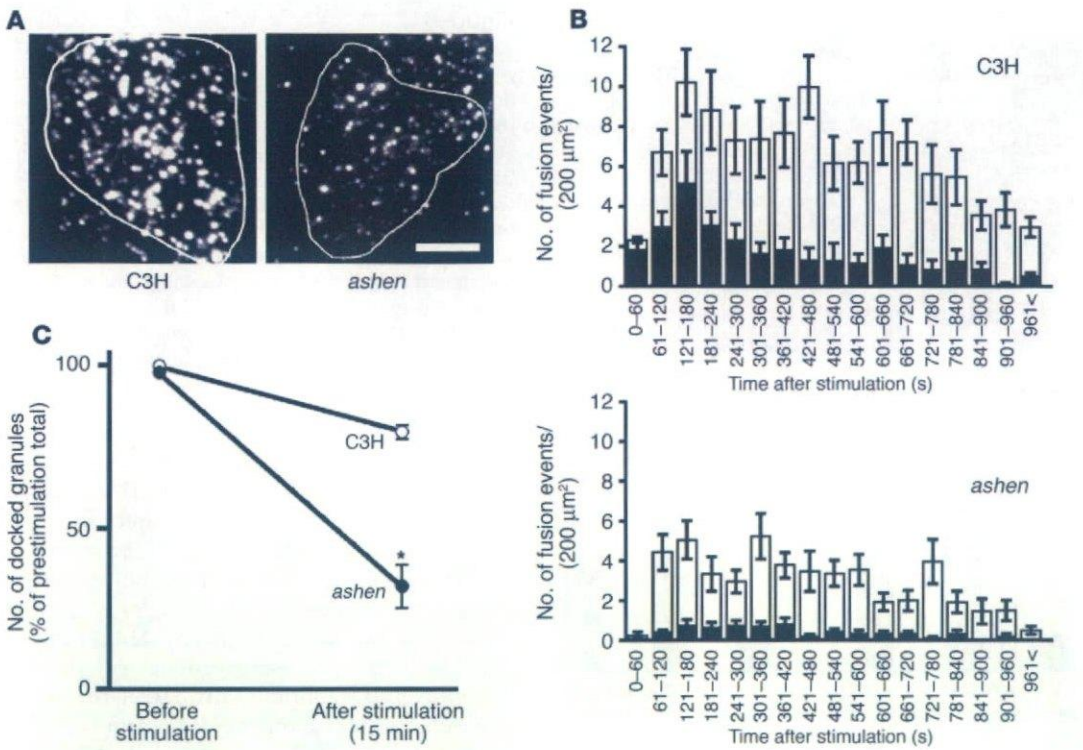

Figure 5

TIRFM analysis of the exocytosis of insulin granules. (**A**) Pancreatic β cells from either C3H/He (left) or *ashen* (right) mice were fixed, immunostained with anti-insulin antibodies, and observed by TIRFM. The surrounding lines represent the outline of cells that are attached to the cover glass. Scale bar: 5 μm. (**B**) Pancreatic β cells of either C3H/He (upper) or *ashen* (lower) mice were infected with adenoviruses encoding insulin-GFP. Evanescent images in live cells were acquired every 300 milliseconds after glucose stimulation. The fusion events per 200 μm² were manually counted. The histograms show the number of fusion events at 60-second intervals after high-glucose (16.7 mM) stimulation. The black bars show the fusion from previously docked granules, whereas the white bars represent that from newly recruited granules. Values are mean ± SE (n = 24 for *ashen* and n = 21 for C3H/He mice). The statistical significance of differences between means were assessed by repeated-measures ANOVA. (**C**) The number of morphologically docked granules was counted on the TIRFM images of pancreatic β cells that had been infected with adenoviruses encoding insulin-GFP. The number after a glucose stimulation (16.7 mM, 15 minutes) was normalized to that prior to the stimulation in the identical area (200 μm²) of C3H/He (open circles) or *ashen* (filled circles) β cells. Values are mean ± SE (n = 4). The statistical significance of differences between means was assessed by Student's t test. *P < 0.0005 vs. C3H/He mice.

fusion events in response to 16.7 mM glucose, however, were significantly decreased (Figure 5B; 15.4 ± 2.5 in 0–5 minutes in *ashen* β cells vs. 34.5 ± 5.6 in 0–5 minutes in C3H/He β cells, P < 0.05; and 32.5 ± 4.2 in 5–16 minutes vs. 72.4 ± 11.5 in 5–16 minutes, P < 0.0001; n = 24 for *ashen* and n = 21 for C3H/He). Remarkably, few fusion events occurred from previously docked granules in *ashen* β cells (5.8 ± 1.3 in 0–16 minutes in *ashen* β cells vs. 26.3 ± 4.3 in 0–16 minutes in C3H/He β cells). The exocytosis of newly recruited granules was relatively modestly affected, although it was also significantly reduced (42.1 ± 4.2 in 0–16 minutes in *ashen* β cells vs. 80.6 ± 11.2 in 0–16 minutes in C3H/He β cells). We then analyzed the changes in the total number of docked granules during glucose stimulation using the TIRFM images. Comparison of the numbers of docked granules in the identical area before and after glucose stimulation should eliminate the effect of potential differences in infection efficiency between cells. The number of docked granules after 15 minutes of glucose stimulation remained 80.3% ± 2.1% of the initial number in the control β cells (Figure 5C). By contrast, it was markedly decreased to 32.1% ± 6.6% in *ashen* β cells, indicating that refilling of the pool of docked granules is defective.

Analysis of insulin granules by EM. We next performed the EM examination of pancreatic β cells from fixative-perfused mice. It did not reveal any obvious alterations in the number, distribution, or appearance (dense-core formation) of granules in *ashen* β cells (data not shown, but see Figure 6A), except that the average diameter was slightly decreased (298 ± 7 nm in *ashen* β cells vs. 322 ± 7 nm in C3H/He β cells, P < 0.05; n = 24 for *ashen* and n = 25 for C3H/He; note that the values represent the mean of the profile diameter in sections but not that of the maximum diameter). To determine whether any of the changes in glucose-stimulated exocytosis identified here are correlated with the finding of EM, islets were first isolated from mice and incubated with either 2.8 mM or 25 mM glucose, and then chemically fixed and subjected to morphometric analysis (Figure 6A). Granules were divided according to the distance from their center to the plasma membrane, and the density of granules in concentric shells below the plasma membrane was calculated relative to the average density of all cytoplasmic granules. Although the density of granules whose centers were located 300–500 nm from the plasma membrane was not significantly different from the average, the density of granules whose centers were located within 100 nm of the plasma membrane was much lower

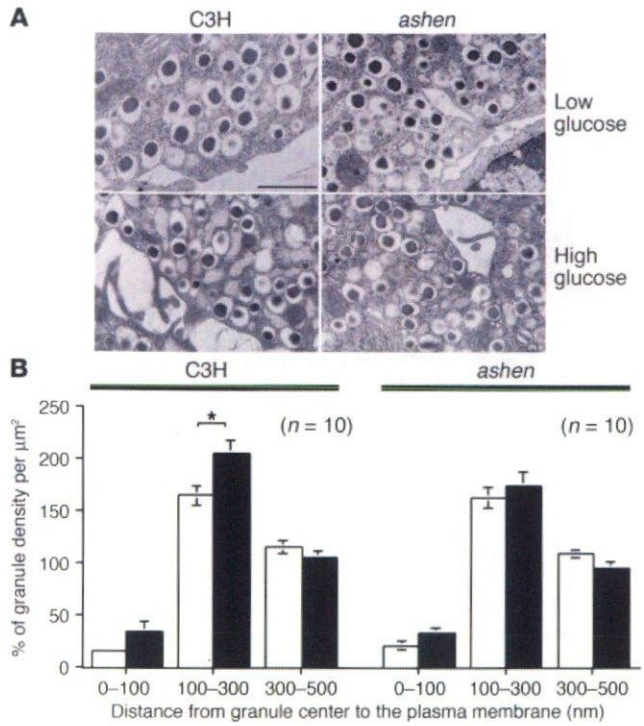

Figure 6
Ultrastructure of the pancreatic β cells. (**A**) Electron micrographs of β cells were taken in nonstimulated (upper) or glucose-stimulated (lower) islets of C3H/He (left) and *ashen* (right) mice. Scale bar: 1 μm. (**B**) Relative density of granules below the plasma membrane in nonstimulated (white bars) or glucose-stimulated (black bars) β cells of C3H/He (left) and *ashen* (right) mice is shown as a function of the distance from granule center to the plasma membrane (nm). Data are represented as a percentage of the granule density in each concentric shell below the plasma membrane relative to the average density in cytoplasm (100% = number of total granules per the area of cytoplasm, that is, the cell area minus the nuclear area). Values are mean ± SE (n = 10). The statistical significance of differences between means was assessed by Student's t test. *P < 0.05.

in both nonstimulated and stimulated control β cells (Figure 6B, left). Given that the diameter of insulin granules is 300–350 nm, which is equivalent to the previously reported value (24), the latter finding is not surprising because the center of granules should not approach the plasma membrane within their radius. By contrast, the density of granules whose centers reside at 100–300 nm significantly increased above the average, which may indicate the accumulation of granules docked onto the plasma membrane. This fraction is thought to correspond to the granules visualized by TIRFM considering the TIRFM coverage area (within 100 nm from the plasma membrane) and the mean diameter of granules (300–350 nm). Interestingly, the density of this fraction was significantly augmented by the exposure to 25 mM glucose in the control β cells. By contrast, the glucose-dependent accumulation of granules beneath the plasma membrane was lacking in *ashen* β cells, although the densities of other fractions were not significantly different from those in the control β cells (Figure 6B, right). These findings suggest that glucose has the ability to replenish a pool of docked granules and that this glucose-driven refilling process is impaired in *ashen* β cells.

Complex formation between granuphilin and syntaxin 1a. We previously demonstrated that the Rab27a effector granuphilin directly interacts with syntaxin 1a, a SNARE protein on the plasma membrane (11), and that wild-type granuphilin, but not its mutants that are defective in binding to either Rab27a or syntaxin 1a, promotes the plasma membrane targeting of insulin granules (12). These findings suggest that granuphilin tethers insulin granules and the plasma membrane through interactions with Rab27a and syntaxin 1a, respectively. To examine the complex formation between granuphilin and syntaxin 1a, coimmunoprecipitation experiments were performed with lysates of isolated islets. Although the expression levels of syntaxin 1a and granuphilin were similar between *ashen* and control islets, the amount of syntaxin 1a coprecipitated with anti-granuphilin antibodies was significantly decreased in *ashen* islets (Figure 7A, lower panel). The reduction was specific, because the amount of another complex containing syntaxin 1a with Munc18-1 (25) was comparable between *ashen* and control islets (Figure 7A, upper panel). This finding is compatible with our previous finding that active Rab27a promotes complex formation between granuphilin and syntaxin 1a (11) and may explain the decreased docking of insulin granules with the plasma membrane in *ashen* β cells. Quantification in independent experiments revealed that the amount of granuphilin/syntaxin 1a complex was reduced to approximately 60% compared with the control (Figure 7B); this value is roughly equivalent to the degree of decrease in the number of docked granules (Figure 5A). The decreased complex formation between syntaxin 1a and granuphilin also indicated that the redistribution of granuphilin to the peripheral plasma membrane region in *ashen* β cells (Figure 1B) is not due to the increased association with syntaxin 1a.

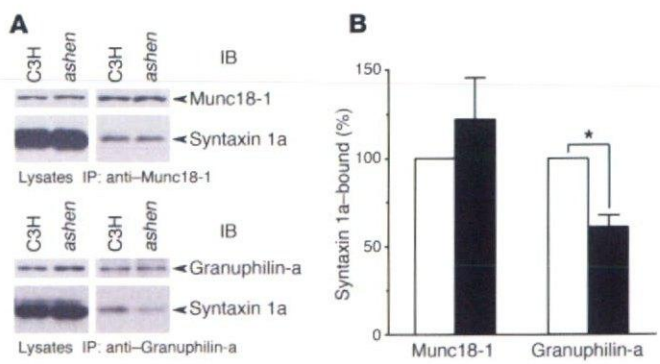

Figure 7
Protein interactions of syntaxin 1a in pancreatic islets. (**A**) Protein interactions of syntaxin 1a with either Munc18-1 (upper) or granuphilin-a (lower) were analyzed in extracts of C3H/He or *ashen* islets. The amount of Munc18-1, granuphilin-a, and syntaxin 1a in each lysate (5 μg, left) and 30–40% of the immunoprecipitates of Munc18-1 or granuphilin-a (right) were examined by immunoblotting with the antibodies indicated. (**B**) Results of coimmunoprecipitation experiments independently performed as described in **A** were gathered for statistics. Relative intensities of syntaxin 1a signals in *ashen* mice (black bars) to those in C3H/He mice (white bars) were calculated and expressed as mean ± SE from 7 (vs. Munc18-1) and 6 (vs. granuphilin-a) immunoblot preparations. When analyzed by a Wilcoxon signed-ranks test, *ashen* islets showed significantly reduced interaction of syntaxin 1a with granuphilin-a (*P = 0.027), but not with Munc18-1.

Discussion

We demonstrate here that insulin secretion in response to a physiological stimulus, glucose, is significantly reduced in *ashen* β cells by 3 independent analyses, which included perifusion, 2-photon excitation imaging, and TIRFM techniques. The possibility of absolute insulin deficiency is excluded because the insulin content in the *ashen* pancreas is slightly elevated. Neither the rise of $[Ca^{2+}]_i$ nor the dynamics of fusion pore opening after a glucose load is altered. These findings indicate that the defect lies in the glucose-stimulated secretory pathway somewhere after the increase in $[Ca^{2+}]_i$ and before the formation of a fusion pore. TIRFM analysis consistently documented reductions in the numbers of docked granules onto the plasma membrane and in the exocytosis from predocked granules. It also showed that docked granules are not efficiently refilled during glucose stimulation in *ashen* β cells. Furthermore, EM analysis revealed the glucose-dependent accumulation of granules beneath the plasma membrane in control β cells, but not in *ashen* β cells. These findings indicate a defect in the replenishment of docked granules during glucose stimulation in *ashen* β cells.

The relatively modest findings by EM compared with those by TIRFM about the differences in the number and refilling of docked granules likely result from technical differences inherent between the 2 methods. TIRFM directly observes the plasma membrane, a fusion site, as a 2-dimensional area of a monolayer cell, although the contact zone with the glass coverslip might be artificially affected by reorganization of the cytoskeleton. On the other hand, EM detects the plasma membrane as a contour of a cell embedded in tissue. Because less than 5% of granules in the section should be released during glucose stimulation when the amount of insulin secreted is estimated relative to the content in cells, it might be difficult to capture resultant morphological changes by EM. Moreover, docked granules themselves may be difficult to identify because there is no specialized docking site like the active zone for synaptic vesicles. It was previously reported that a population of docked granules can be identified by EM only in unfixed, quickly frozen cells (26). Even by using such cryopreservation methods, however, there are discrepant findings concerning the accumulation and preferential exocytosis of morphologically docked granules in chromaffin cells (26, 27). Despite these technical differences and difficulties, our TIRFM and EM findings indicate that the dysfunction of Rab27a affects glucose-driven refilling of docked granules and thus reduces glucose-induced exocytosis in both early and late phases. This notion is further corroborated by the perifusion data that insulin secretion is significantly decreased at each of the repeated exposures to the glucose stimuli in *ashen* β cells.

In contrast to glucose stimulation, *ashen* β cells do not reveal any decrease of insulin secretion in response to high K^+, whether it is given once or repeatedly, or in response to other pharmacological enhancers. Although disturbance of vesicle transport by alteration of Rab protein is not surprising, the secretagogue-specific defect in exocytosis identified here was unexpected. What mechanism is underlying this phenomenon? It is unlikely that glucose metabolism itself is impaired by the Rab27a mutation. Indeed the amplitude and time course of $[Ca^{2+}]_i$ increase in response to glucose, which is dependent on ATP generation through glucose metabolism, is indistinguishable between *ashen* and control β cells. Furthermore, high K^+– and glucose-induced insulin secretion measured in the presence of diazoxide, which is thought to reflect a pathway amplified by glucose metabolism (19, 20), is largely intact in *ashen* β cells. These findings indicate that the suppression of glucose-stimulated insulin secretion does not involve an effect on glucose metabolism per se. Although both high K^+ and glucose induce membrane depolarization and subsequent Ca^{2+} influx through activation of voltage-dependent Ca^{2+} channels in pancreatic β cells, the mechanism for inducing depolarization is different. High K^+ induces it physically, whereas glucose does so by closing K_{ATP} channels through the ATP production. Accordingly, the 2 stimuli elicit distinct patterns and time courses of $[Ca^{2+}]_i$ change (20, 24). High K^+ elicits a large but transient peak of elevated $[Ca^{2+}]_i$, which returns spontaneously towards the prestimulatory level despite the continuous presence of high K^+, whereas glucose induces a biphasic response in $[Ca^{2+}]_i$, consisting of an initial large increase and long-lasting oscillations that remain throughout the glucose application. These distinct $[Ca^{2+}]_i$ changes might differentially affect the action of Rab27a and its effectors by influencing protein-protein or protein-lipid interactions. Another possibility is that glucose generates signals other than $[Ca^{2+}]_i$ that act on the Rab27a system. It has recently been reported that glucose-induced reduction of the cytoplasmic ADP concentration activates phosphatidylinositol 4-kinase activity in pancreatic β cells and that the resultant increase in phosphoinositides enhances the number of releasable granules (28). The production of phosphoinositides on the plasma membrane might recruit Rab27a effectors because many of them contain C2 domains that have potential affinity to these lipids (1, 6).

The function of Rab27a in the docking process of insulin granules is consistent with the known property of granuphilin, a principal Rab27a effector in pancreatic β cells. It has been shown that granuphilin directly binds to the plasma membrane-anchored SNARE, syntaxin 1a, and that active Rab27a enhances the complex formation in the β cell line MIN6 (11). Furthermore, wild-type granuphilin, but not its mutants that are defective in binding to Rab27a or syntaxin 1a, promotes the plasma membrane targeting of insulin granules (12). Moreover, previous TIRFM analysis has shown that insulin granules are preferentially docked to syntaxin 1a clusters in the intact plasma membrane of MIN6 cells (29). The correlated reductions in the docking of granules and the complex formation in *ashen* β cells, shown here, further support a role of the interaction between granuphilin and syntaxin 1a in the docking process. It is possible, however, that granuphilin also mediates this process by other mechanisms. As described above, its C-terminal C2 domains may contribute to the docking process through an affinity to membrane phospholipid, because granuphilin appears to associate with the plasma membrane even when its interaction with syntaxin 1a is decreased in *ashen* β cells.

In summary, the present study has provided the first genetic documentation to our knowledge for the role of Rab27a in the exocytosis of secretory granules. It also has given an insight into physiological aspects of insulin secretion. Our findings suggest that glucose promotes the replenishment of a pool of docked granules by using the activity of Rab27a. The defect in the docking of granules in *ashen* β cells is reminiscent of the finding that *ashen* lytic granules do not reach the plasma membrane at the immunological synapse, although they are polarized to the target cell interface (14). There is, however, a marked difference between the 2 organelles in terms of their efficiencies of exocytosis. Although *ashen* lytic granules are almost incapable of subsequent fusion (13, 14), *ashen* secretory granules are substantially released. The significance of Rab27a in physiological insulin secretion is supported by the

in vivo glucose intolerant phenotype of *ashen* mice. Patients with Griscelli syndrome may also exhibit glucose intolerance, although most of them die in childhood from hemophagocytotic syndrome without bone-marrow transplantation (30).

Methods

Mice, phenotypic characterization, and tissue preparation. All animal experiments were performed in accordance with the rules and regulations of the Animal Care and Experimentation Committee, Gunma University, Showa Campus. The *ash/ash* (C3H/He background) and control C3H/He mice were kindly provided by N.A. Jenkins (National Cancer Institute, Frederick, Maryland, USA). All mice were weaned at 4 weeks of age and had free access to water and standard laboratory chow (CE-2; CLEA Japan) in an air-conditioned room with a 12-hour light/12-hour dark cycle. An intraperitoneal glucose tolerance test (1 g glucose/kg body weight) and an intraperitoneal insulin tolerance test (0.75 U human insulin/kg body weight) were performed as described previously (18). Blood glucose levels were determined by a glucose oxidase method using Glutest sensor and Glutest Pro GT-1660 (Sanwa Kagaku Kenkyujyo). The plasma insulin concentration was measured by a LBIS mouse insulin ELISA kit (U-type; Shibayagi Co.). For the measurement of insulin content, the pancreata were excised and weighed, and each was then cut into small pieces and frozen by liquid nitrogen. Insulin was extracted by homogenization using a glass-Teflon homogenizer (1,300 rpm, 30 strokes) in an acid-ethanol solution (70% ethanol and 0.18 M HCl) and then by sonication for 20 seconds. After centrifugation at 3,000 *g* for 10 minutes, the immunoreactive insulin in the supernatant was measured as described previously (31).

Immunoblotting and immunostaining analyses. Rabbit anti-granuphilin antibodies, αGrp-aC that recognizes granuphilin-a (10) and αGrp-N that recognizes both granuphilin-a and -b (9), and rabbit anti-Rab27b antibodies against glutathione-*S*-transferase–fused mouse Rab27b protein (16) were previously described and characterized. Mouse anti-Rab27a and anti–α-tubulin monoclonal antibodies were purchased from BD Biosciences — Pharmingen and Sigma-Aldrich, respectively. Immunoblotting and immunostaining analyses were performed as described previously (16).

Perifusion assays in isolated islets. Islets were isolated from cervically dislocated mice by pancreatic duct injection of 500 U/ml of collagenase solution (type XI; Sigma-Aldrich) followed by digestion at 37°C for 30 minutes with mild shaking, as described previously (31). Islets were picked up by hand selection under a dissecting microscope and cultured overnight in RPMI 1640 medium (11 mM glucose) supplemented with 7.5% fetal calf serum, 100 units/ml penicillin, and 100 μg/ml streptomycin. Thirty islets were placed at the bottom of a 1-ml syringe that had been cut to a volume of 400 μl and plugged with cotton. They were perifused with low-glucose Krebs-Ringer buffer (15 mM HEPES [pH 7.4], 120 mM NaCl, 5 mM KCl, 2 mM $CaCl_2$, 1 mM $MgCl_2$, 24 mM $NaHCO_3$, 0.1% bovine serum albumin, and 2.8 mM glucose) at a constant flow rate of 1.0 ml/min for 30 minutes. After this stabilization period, they were further perifused with the same buffer for 10 minutes followed by the buffer containing various secretagogues.

For glucose stimulation, islets were perifused with the high-glucose buffer (16.7 mM) for 30 minutes, followed by that containing 2.8 mM glucose for 20 minutes. For stimulation by high K^+ concentration, islets were perifused with buffer containing 60 mM KCl plus 65 mM NaCl, 30 mM KCl plus 95 mM NaCl, or 20 mM KCl plus 105 mM NaCl for 15 minutes, followed by the standard buffer for 15 minutes. For the application of forskolin (Sigma-Aldrich) or PMA (Calbiochem-Novabiochem), islets were perifused in the continuous presence of either drug with the standard buffer for 15 minutes, then with the high-glucose buffer for 20 minutes, with the standard buffer for 15 minutes, and were finally perifused without the drug for 10 minutes. For repeated stimulation, the islets were perifused with the standard buffer and then stimulated 4 times by either the high-glucose buffer for 20 minutes or the buffer containing 60 mM KCl plus 65 mM NaCl for 10 minutes, with 10-minute intervals using the standard buffer. For the effect of diazoxide (Sigma-Aldrich), islets were perifused with Krebs-Ringer buffer containing 250 μM diazoxide and 16.7 mM glucose for 50 minutes. They were further perifused in the same buffer for 10 minutes, followed with the buffer containing 30 mM kCl plus 95 mM NaCl for 30 minutes, then with the prestimulation buffer for 15 minutes, in the continuous presence of diazoxide and glucose. All of the perifusate solution was equilibrated with 95% O_2 and 5% CO_2 and maintained at 37°C. Fractions were collected every 1 minute, and the insulin secretion was measured.

Two-photon excitation imaging of exocytotic events in pancreatic islets. Exocytotic events of insulin granules inside living pancreatic islets were visualized with a solution containing a fluid-phase tracer, sulforhodamine B, using 2-photon excitation imaging, as described previously (21). Exocytotic events in response to glucose (20 mM) were measured within an arbitrary area (2,000 μm^2) of islets. The dynamics of fusion pore opening were examined by measuring latency for the onset of staining with sulforhodamine B (1.4 nm) relative to that of staining with 10-kDa fluorescein-dextran (6 nm). The cytosolic Ca^{2+} concentration was measured using Fura-2 acetoxymethyl ester (Molecular Probes) as described previously (21).

TIRFM analysis of pancreatic β cells. Analysis by TIRFM was performed using an inverted microscope (IX70; Olympus) with a high-aperture objective lens (Apo ×100 OHR, NA 1.65; Olympus) as described previously (23). Briefly, isolated islets were dissociated into single cells by incubation in Ca^{2+}-free Krebs-Ringer buffer containing 1 mM EDTA and cultured on fibronectin-coated (Koken Co. Ltd.) high-refractive-index glass (Olympus). For immunocytochemical analysis, the cells were fixed and made permeable with 2% paraformaldehyde and 0.1% Triton X-100. For the observation of fusion events of GFP-labeled insulin granules, the cells were infected by adenovirus encoding GFP-tagged insulin (Adex1CA insulin-GFP).

EM analysis. Animals were anesthetized with sodium pentobarbital and fixed by perfusion with 100 ml of 2% paraformaldehyde and 2% glutaraldehyde in 0.1 M cacodylate buffer, pH 7.4, at 4°C, followed by perfusion with 10 ml of 0.86% saline solution. The pancreas was immersed in the same fixative for 3 hours at 4°C and dissected into small blocks. The blocks containing pancreatic islets were further immersed into 10% sucrose in the cacodylate buffer for 1 hour at 4°C. They were then postfixed with 2% osmium tetroxide in the cacodylate buffer for 1.5 hours at 4°C, dehydrated, infiltrated, and embedded in plastic resin. Ultrathin sections (90 nm) were cut on an Ultracut E ultramicrotome (Reichert-Jung), stained with uranyl acetate and lead citrate, and analyzed by a JEM 1010 electron microscope (JEOL).

For morphometric analysis, islets were isolated from mice by collagenase digestion and cultured overnight. They were then incubated in Krebs-Ringer buffer containing 2.8 mM glucose at 37°C for 1 hour (nonstimulated islets), and some of them were further incubated in the buffer containing 25 mM glucose for 30 minutes (stimulated islets). Both types of islet were fixed by immersion with 2% paraformaldehyde/2% glutaraldehyde/0.2% picric acid in 0.1 M cacodylate buffer, pH 7.4 for 1.5 hours at room temperature and embedded into 1% agarose. They were then postfixed, embedded in plastic resin, and sectioned as described above. Micrographs were randomly taken at ×5,000 and ×8,000 magnifications and captured with an image scanner (CC-500L, Epson) at 720 dots per inch. The entire cell circumference was included, and 10 individual β cells derived from 2 mice were analyzed for each condition. The images at ×5,000 magnification were used to measure the area of cytoplasm and the perimeter of the plasma membrane by ImageJ program (http://rsb.info.nih.gov/ij), whereas those at ×8,000 magnification were used to count granules. The center of granules

was determined and the number of granules located in concentric shells at increasing distance from the plasma membrane (100- or 200-nm thick as indicated) was counted.

Coimmunoprecipitation experiments. The isolated islets were placed in glucose-free Dulbecco's modified Eagle medium (2.8 mM glucose) supplemented with 10% fetal calf serum and frozen at −80°C until the cell lysis. Protein was extracted from 400–600 islets in 1 μl per islet of lysis buffer containing 20 mM Tris (pH 7.5), 150 mM NaCl, 2 mM $MgCl_2$, 1 mM EGTA, 1.0% or 0.2% Triton-X 100, and 1 × protease inhibitor cocktail (Complete mini; Roche Diagnostics). After removal of insoluble materials by centrifugation at 15,000 rpm for 30 minutes, the extracts were incubated with 30 μl of a 50% slurry of protein G-Sepharose (Amersham Biosciences) for 3–4 hours at 4°C under gentle rotation, and then centrifuged at 7,000 rpm for 3 minutes. The precleared extracts were then incubated with 5 μl of anti-Munc18 serum (Synaptic Systems) or αGrp-aC overnight at 4°C. The immune complexes were captured by an addition of 15 μl of 50% protein G-Sepharose for 2 hours at 4°C. Immunoprecipitates were washed 4 times with lysis buffer and finally dissolved in SDS-sample buffer. Immunoprecipitates and original precleared protein extracts were separated by SDS-polyacrylamide gel electrophoresis and were transferred onto an Immobilon-P membrane (Millipore). Protein interactions of syntaxin 1a with Munc18-1 or with granuphilin-a were analyzed by immunoblotting with anti-syntaxin 1a mouse monoclonal antibodies (HPC-1, 1:3,000 dilution; Sigma-Aldrich). The amount of Munc18-1 or granuphilin-a in each immunoprecipitate was evaluated by immunoblot analysis using anti-Munc18 mouse monoclonal antibodies (1:300 dilution; BD Biosciences – Pharmingen) and αGrp-N (1:2,000 dilution). Chemiluminescent signals on the x-ray film were captured with a scanner and quantified using Gel Plotting Macros of NIH Image 1.62 program (http://rsb.info.nih.gov/nih-image).

Statistical analysis. Most analyses comparing the average between 2 groups were done by Student's *t* test. Perifusion data were analyzed by repeated-measures ANOVA. Immunoblot signals were analyzed by a Wilcoxon signed-ranks test.

Acknowledgments

We thank T. Takeuchi, S. Torii, H. Yokota-Hashimoto, H. Takemura, T. Ishizaka, N. Satoh (Gunma University), and C. Nishiwaki (Kyorin University) for generous support. This work was supported by grants-in-aid for scientific research and the 21st Century Center of Excellence Program from the Ministry of Education, Culture, Sports, Science, and Technology of Japan. It was also supported by grants from the Takeda Science Foundation, The Naito Foundation, the Daiwa Securities Health Foundation, and by a Japan Insulin Study Group Award (to T. Izumi).

Received for publication August 6, 2004, and accepted in revised form November 16, 2004.

Address correspondence to: Tetsuro Izumi, Department of Molecular Medicine, Institute for Molecular and Cellular Regulation, Gunma University, 3-39-15 Showa-machi, Maebashi, Gunma 371-8512, Japan. Phone: 81-27-220-8856; Fax: 81-27-220-8860; E-mail: tizumi@showa.gunma-u.ac.jp.

1. Izumi, T., Gomi, H., Kasai, K., Mizutani, S., and Torii, S. 2003. The roles of Rab27 and its effectors in the regulated secretory pathways. *Cell Struct. Funct.* **28**:465–474.
2. Tolmachova, T., et al. 2004. A general role for Rab27a in secretory cells. *Mol. Biol. Cell.* **15**:332–344.
3. Söllner, T.H. 2003. Regulated exocytosis and SNARE function. *Mol. Membr. Biol.* **20**:209–220.
4. Blott, E.J., and Griffiths, G.M. 2002. Secretory lysosomes. *Nat. Rev. Mol. Cell Biol.* **3**:122–131.
5. Nagashima, K., et al. 2002. Melanophilin directly links Rab27a and myosin Va through its distinct coiled-coil regions. *FEBS Lett.* **517**:233–238.
6. Kuroda, T.S., Fukuda, M., Ariga, H., and Mikoshiba, K. 2002. The Slp homology domain of synaptotagmin-like proteins 1-4 and Slac2 functions as a novel Rab27A binding domain. *J. Biol. Chem.* **277**:9212–9218.
7. Ménasché, G., et al. 2000. Mutations in *RAB27A* cause Griscelli syndrome associated with haemophagocytic syndrome. *Nat. Genet.* **25**:173–176.
8. Wilson, S.M., et al. 2000. A mutation in *Rab27A* causes the vesicle transport defects observed in *ashen* mice. *Proc. Natl. Acad. Sci. U. S. A.* **97**:7933–7938.
9. Yi, Z., et al. 2002. The Rab27a/granuphilin complex regulates the exocytosis of insulin-containing dense-core granules. *Mol. Cell. Biol.* **22**:1858–1867.
10. Wang, J., Takeuchi, T., Yokota, H., and Izumi, T. 1999. Novel rabphilin-3-like protein associates with insulin-containing granules in pancreatic beta cells. *J. Biol. Chem.* **274**:28542–28548.
11. Torii, S., et al. 2002. Granuphilin modulates the exocytosis of secretory granules through the interaction with syntaxin 1a. *Mol. Cell. Biol.* **22**:5518–5526.
12. Torii, S., Takeuchi, T., Nagamatsu, S., and Izumi, T. 2004. Rab27 effector granuphilin promotes the plasma membrane targeting of insulin granules via interaction with syntaxin 1a. *J. Biol. Chem.* **279**:22532–22538.
13. Haddad, E.K., Wu, X., Hammer, J.A., III, and Henkart, P.A. 2001. Defective granule exocytosis in Rab27a-deficient lymphocytes from *ashen* mice. *J. Cell Biol.* **152**:835–841.
14. Stinchcombe, J.C., et al. 2001. Rab27a is required for regulated secretion in cytotoxic T lymphocytes. *J. Cell Biol.* **152**:825–833.
15. Barral, D.C., et al. 2002. Functional redundancy of Rab27 proteins and the pathogenesis of Griscelli syndrome. *J. Clin. Invest.* **110**:247–257. doi:10.1172/JCI200215058.
16. Zhao, S., Torii, S., Yokota-Hashimoto, H., Takeuchi, T., and Izumi, T. 2002. Involvement of Rab27b in the regulated secretion of pituitary hormones. *Endocrinology.* **143**:1817–1824.
17. Wu, X.S., et al. 2002. Identification of an organelle receptor for myosin-Va. *Nat. Cell Biol.* **4**:271–278.
18. Hirayama, I., et al. 1999. Genetic analysis of obese diabetes in the TSOD mouse. *Diabetes.* **48**:1183–1191.
19. Aizawa, T., Komatsu, M., Asanuma, N., Sato, Y., and Sharp, G.W.G. 1998. Glucose action 'beyond ionic events' in the pancreatic β cells. *Trends Pharmacol. Sci.* **19**:496–499.
20. Henquin, J.-C. 2000. Triggering and amplifying pathways of regulation of insulin secretion by glucose. *Diabetes.* **49**:1751–1760.
21. Takahashi, N., Kishimoto, T., Nemoto, T., Kadowaki, T., and Kasai, H. 2002. Fusion pore dynamics and insulin granule exocytosis in the pancreatic islet. *Science.* **297**:1349–1352.
22. Steyer, J.A., and Almers, W. 2001. A real-time view of life within 100 nm of the plasma membrane. *Nat. Rev. Mol. Cell Biol.* **2**:268–276.
23. Ohara-Imaizumi, M., et al. 2004. TIRF imaging of docking and fusion of single insulin granule motion in primary rat pancreatic β-cells: different behaviour of granule motion between normal and Goto-Kakizaki diabetic rat β-cells. *Biochem. J.* **381**:13–18.
24. Olofsson, C.S., et al. 2002. Fast insulin secretion reflects exocytosis of docked granules in mouse pancreatic B-cells. *Pflugers Arch.* **444**:43–51.
25. Hata, Y., Slaughter, C.A., and Südhof, T.C. 1993. Synaptic vesicle fusion complex contains *unc-18* homologue bound to syntaxin. *Nature.* **366**:347–351.
26. Steyer, J.A., Horstmann, H., and Almers, W. 1997. Transport, docking and exocytosis of single secretory granules in live chromaffin cells. *Nature.* **388**:474–478.
27. Plattner, H., Artalejo, A.R., and Neher, E. 1997. Ultrastructural organization of bovine chromaffin cell cortex: analysis by cryofixation and morphometry of aspects pertinent to exocytosis. *J. Cell Biol.* **139**:1709–1717.
28. Olsen, H.L., et al. 2003. Phosphatidylinositol 4-kinase serves as a metabolic sensor and regulates priming of secretory granules in pancreatic β cells. *Proc. Natl. Acad. Sci. U. S. A.* **100**:5187–5192.
29. Ohara-Imaizumi, M., et al. 2004. Site of docking and fusion of insulin secretory granules in live MIN6 β cells analyzed by TAT-conjugated anti-syntaxin 1 antibody and total internal reflection fluorescence microscopy. *J. Biol. Chem.* **279**:8403–8408.
30. Klein, C., et al. 1994. Partial albinism with immunodeficiency (Griscelli syndrome). *J. Pediatr.* **125**:886–895.
31. Izumi, T., et al. 2003. Dominant negative pathogenesis by mutant proinsulin in the Akita diabetic mouse. *Diabetes.* **52**:409–416.

GLIA 52:98–107 (2005)

Involvement of β1 Integrin in Microglial Chemotaxis and Proliferation on Fibronectin: Different Regulations by ADP Through PKA

KAORU NASU-TADA,[1] SCHUICHI KOIZUMI,[1] AND KAZUHIDE INOUE[2,3]*
[1]*Division of Pharmacology, National Institute of Health Sciences, Setagaya, Tokyo, Japan*
[2]*Division of Biosignaling, National Institute of Health Sciences, Setagaya, Tokyo, Japan*
[3]*Graduate School of Pharmaceutical Sciences, Kyushu University, Higashi-ku, Fukuoka, Japan*

KEY WORDS
PKA; ATP; ADP; purinergic; glia; extracellular matrix; migration

ABSTRACT
Microglia are immune cells in the brain; their activation, migration, and proliferation have pivotal roles in brain injuries and diseases. Microglia are known to attach firmly to fibronectin, the upregulation of which is associated with several pathological conditions in the CNS, through β1 integrin and become activated. Extracellular nucleotides can serve as potent signaling molecules. Recently, ATP and ADP were revealed to possess chemoattractive properties to microglia via Gi-coupled P2Y receptors. In the present study, we report that the ADP-induced chemotaxis of microglia is mediated by P2Y12/13 receptors and is β1 integrin-dependent in the presence of fibronectin. Signals from P2Y12/13 receptors also cause β1 integrin translocation to the membrane ruffle regions, but this redistribution was lost when the intracellular cyclic AMP (cAMP) was increased by forskolin or dibutyryl cAMP. This inhibitory effect of cAMP-elevating agents did not appear when microglia were co-incubated with a protein kinase A (PKA) inhibitor, KT-5720, suggesting that PKA is a negative regulator of the β1 integrin translocation. We also show that the engagement of β1 integrin enhanced microglial proliferation. Signals from P2Y12/13 receptors attenuated the proliferation, whereas ADP itself had no effect on microglial growth. Furthermore, β1 integrin-induced proliferation is positively regulated by the cAMP-dependent PKA. Together, these results indicate the involvement of β1 integrin in microglial proliferation and chemotaxis, both of which have clinical importance. The data also suggest that PKA is inversely involved in these two cellular functions.

INTRODUCTION

Microglia are considered to act as brain macrophages. They participate in brain injuries and diseases (Nakajima and Kohsaka, 1993), in which their motility, aberrant activation, and proliferation are known to play crucial roles. Microglia quickly respond to numerous inflammatory mediators by migrating to the source of the mediators, where they become activated and exert their neuroprotective effects (Hanisch, 2002; Streit, 2002). Unfortunately, their hyperactivation often leads to neurotoxicity instead, and several pathological conditions in the CNS are, in fact, accompanied by an excess proliferation of microglia (Gehrmann et al., 1995). Thus, better understanding of the regulation of microglial chemotaxis and proliferation may have important therapeutic implications.

Integrins are heterodimeric transmembrane proteins consisting of α and β subunits; they mediate cell–cell and cell–extracellular matrix (ECM) interactions. At present, 16 α and 8 β chains have been identified, and at least 22 different complexes are known. β1 integrin, the most ubiquitous β subunit, pairs with at least 10 different α chains to comprise receptors for a wide variety of ECM proteins. Within the CNS, β1 integrin is expressed on many different cell types, including neurons, glial cells, and endothelial cells (Pinkstaff et al., 1999). As shown previously by other investigators, microglia express several integrin receptors of β1 and β2 families that are upregulated following microglial activation in vitro (Hailer et al., 1996; Yu et al., 1998; Kloss et al., 2001; Milner and Campbell, 2003). In vivo, integrin expression is found to be increased on activated microglia in Alzheimer's disease (Akiyama and McGeer, 1990), after nerve injuries (Coyle, 1998; Kloss et al., 1999; Tsuda et al., 2003) and in multiple sclerosis lesions (Bo et al., 1996). Integrins serve not only as adhesive molecules but also as signaling receptors, and they regulate numerous cellular functions (Hemler, 1998) including cell migration and proliferation. β1 integrin is closely associated with the regulation of cell motility and growth in many cell types (Hynes, 1992; Jones and Watt, 1993; Howlett et al., 1995), but its role in microglial chemotaxis and proliferation remains unclear.

Fibronectin is one of the ECM molecules; it is a large, multidomain glycoprotein that exists both as a cell surface protein and in plasma. The expression of ECM molecules is regionally and developmentally regulated in the brain, and their presence is relatively minor in the

*Correspondence to: Kazuhide Inoue, Department of Molecular and System Pharmacology, Graduate School of Pharmaceutical Sciences, Kyushu University, 3-1-1 Maidashi, Higashi-ku, Fukuoka 812-8582, Japan.
E-mail: inoue@phar.kyushu-u.ac.jp

Received 16 December 2004; Accepted 24 March 2005

DOI 10.1002/glia.20224

Published online 26 May 2005 in Wiley InterScience (www.interscience.wiley.com).

normal CNS. Some ECM molecules, including fibronectin, however, are upregulated after adult CNS injury. Fibronectin also exists at high concentrations in the blood plasma and a breakdown of the blood-brain barrier should result in an increase in its local concentration in the CNS. Fibronectin induces firm adhesion and activation of microglia (Milner and Campbell, 2002, 2003). It is a major ligand of the β1 integrin family, but recently Mac-1 was also reported to play a role in the adhesion of leukocytes to fibronectin (Lishko et al., 2003).

Previously, Honda et al. (2001) demonstrated that extracellular ATP and ADP could induce the chemotactic migration of microglia. Several lines of evidence so far have indicated that extracellular nucleotides serve as signaling molecules (Bodin and Burnstock, 2001). ATP, and possibly other nucleotides, are released from damaged cells or secreted via nonlytic mechanisms and activate microglia. In the work by Honda et al. (2001), extracellular ATP and ADP induced chemotaxis as well as membrane ruffling, which was possibly mediated by Gi-coupled P2Y receptors. The P2Y12 receptor is a recently cloned Gi-coupled P2 receptor (Hollopeter et al., 2001), and expressed on platelets and exclusively in microglia in the brain (Sasaki et al., 2003). The P2Y13 receptor is another Gi-coupled P2 receptor that was recently identified (Communi et al., 2001; Zhang et al., 2002). Its messenger RNA is expressed at highest levels in the brain and immune tissues, particularly the spleen (Zhang et al., 2002), suggesting its roles in neuron and in immune systems. P2Y12 and P2Y13 receptors present a very similar pharmacological profile. Both receptors show high affinities for ADP and 2MeSADP (Hollopeter et al., 2001; Zhang et al., 2002) and are selectively blocked by ARC-67085 and ARC-69931 (Ingall et al., 1999). No specific agonists/antagonists are known currently to distinguish these two receptors pharmacologically.

The involvement of β1 integrin in chemotaxis and proliferation is already well characterized. Its role in microglial chemotaxis and proliferation, however, has not been well studied, and its correlation with purinoceptors such as P2Y12/13 receptor is still unclear. We provide new evidence that (1) ADP-induced chemotaxis through P2Y12/13 receptors involves β1 integrin in the presence of fibronectin, (2) ADP induces β1 integrin redistribution which colocalizes with membrane ruffling on microglia, and PKA functions as a negative regulator of this translocation, (3) β1 integrin mediates microglial proliferation through positive regulation of PKA, and (4) signals from P2Y12/13 receptors abrogate the proliferative effect of β1 integrin. Taken together, these results indicate that β1 integrin is crucially involved in both the proliferation and chemotaxis of microglia, which are under the inverse regulation of PKA.

Abbreviations

ATP	adenosine 5′-triphosphate
ADP	adenosine 5′-diphosphate
cAMP	adenosine 2′:3′-cyclic monophosphate
CNS	central nervous system
CCR	CC chemokine receptor
CXCR	CXC chemokine receptor
CX_3CR	CX_3C chemokine receptor
ECM	extracellular matrix
ERK	extracellular signal-regulated kinase
GPCR	G-protein-coupled receptor
IL-8	interleukin-8
MAP	mitogen-activated protein
2MeSADP	dimethylthioadenosine 5′-diphosphate
PKA	protein kinase A
VLA	very late antigen

MATERIALS AND METHODS

Isolation of Microglia

Rat primary cultures were derived from the cerebral cortex of neonatal Wistar rats. In brief, the rat cortices were separated from the meninges, minced, treated with trypsin and DNase, and then centrifuged to remove dead cells. The pellet was resuspended in DMEM, filtrated and cultured in medium with 10% fetal bovine serum for 12–23 days. Microglia were isolated on day 10 and day 15 by gently shaking of the flasks for 2 min and were attached to appropriate dishes or coverslips. One flask (75 cm^2) yielded 1–2 × 10^6 microglial cells by this preparation, and the cultures were of >98% purity. The purity of microglial culture was determined by immunostaining for Ox-42 and Eva-1.

Immunofluorescence Staining of Cell Surfaces

Microglia were washed once with ice-cold staining buffer [phosphate-buffered saline (PBS) 1% fetal calf serum (FCS), 0.1% NaN_3] and then Fc blocked for 15 min on ice. After washing, they were incubated with Ha2/5 (PharMingen) for 30 min on ice. They were washed once, incubated with mouse anti-hamster IgM (PharMingen) for 30 min on ice, and then washed again. Finally, cells were incubated with Alexa-Fluor 488-conjugated anti-mouse IgG (Molecular Probes, Eugene, OR) for 30 min on ice in the dark, washed twice, resuspended in the staining buffer, and the fluorescence intensity of the labeled microglia was analyzed with FACScan (Becton Dickinson).

Immunocytochemistry

Coverslips were briefly treated with hydrochloric acid and extensively washed with PBS. They were then coated with fibronectin (Sigma, St. Louis, MO) at 10 μg/ml overnight and washed with PBS immediately before use. Microglia were plated on coverslips and kept at 37°C for 1 h, and unattached cells were washed off gently with warm DMEM. After 1-h serum starvation, the cells were stimulated with ADP (50 μM) for 5 min at 37°C. The attached cells were then fixed in 3.7% formaldehyde in PBS for 5 min and then washed with PBS. The cells were permeabilized with 0.1% Triton-X in PBS for 5 min, washed again with PBS, and then blocked for 30 min with ACE blockase (Yukijirushi, Ltd.) with 3% goat serum at room temperature. To visualize β1 integ-

rin and membrane ruffling, the cells were stained with Ha2/5 mAb, mouse anti-hamster IgM Ab, Alexa-Fluor 488-conjugated goat anti-mouse IgG, or Texas Red-X phalloidin (Molecular Probes) and observed under a fluorescent microscope.

Defining Membrane Rufflings

To the best of our knowledge, there are no methods to quantify the degree of membrane ruffling. Therefore, we tried to define membrane ruffling by analyzing the pictures from immunocytochemistry. First we pictured cells that were stained with Texas Red-X phalloidin, and then a line was drawn across the cell and the intensity of the Texas Red-X phalloidin labeling along the line was analyzed using computer software. Membrane ruffling is characterized by the sharp, strong labeling of Texas Red-X phalloidin, which reaches >200 a.u. (out of 256) of intensity, whereas cells with no ruffling show less intense, blurred, and dispersed staining. We defined membrane ruffling as a wave-like structure that is stained with phalloidin and the labeling intensity of which reaches >200 a.u.. Cells satisfying these criteria were construed as bearing membrane ruffling morphology.

Chemotaxis Assay

Chemotaxis assays were performed using a direct-viewing Dunn chemotaxis chamber (Weber Scientific International, Teddington, UK). The details concerning this apparatus and its use are given in Webb et al. (1996) and Zicha et al. (1991). In brief, microglia were attached to coverslips that had been coated with fibronectin. After 1-h incubation, the cells were washed with warm DMEM and cultured in the absence of FCS for an additional 1 h. The coverslips were then inverted onto the slide, the inner and the outer wells of which were filled with DMEM. The edges of the coverslip were tightly sealed with adhesive tape except for one on which a thin filling slit was left. Using a needle and a syringe, the medium in the outer well was gently replaced with DMEM containing 100 μM ADP. The filling slit was quickly sealed with adhesive tape and the chamber was carefully set on the stage of a microscope equipped with a 10× phase-contrast objective. Microglia adhered to the coverslip were exposed to the ADP gradient and then monitored in the Dunn chemotaxis chamber for a period of 1 h. One region of the bridge was viewed directly via a CCD video camera and the data were recorded every 30 s during the 1-h observation using image software. After recording, cells were randomly selected from a set area of the field and the straight distance they migrated was plotted against x,y coordinates on scatter diagrams. The x-axis was parallel to the outer ring while the y-axis was vertical. Recording of the cell migration usually started within 30 min of assembling the chamber, by which time a linear diffusion gradient had been established (Webb et al., 1996).

Proliferation Assay

In this study, 96-well plates (Corning) were incubated with fibronectin (10 μg/ml), anti-β1 integrin Ab (10 μg/ml) (Santa Cruz Biotechnology, Santa Cruz, CA) or normal rabbit serum (Sigma) overnight at 4°C and washed with PBS before use. For anti-β1 integrin Ab and normal rabbit serum coatings, the wells were pre-coated with goat anti-rabbit IgG (Sigma) for 2 h at 37°C and washed with PBS. Microglia were attached to the wells and cultured in DMEM 4% FCS for 24 h at 37°C. After the incubation, cell survival and proliferation were assayed using an MTT cell growth kit (Chemicon) according to the manufacturer's instructions and also by direct cell counting.

RESULTS

ADP-Induced Chemotaxis of Microglia Is Mediated by P2Y12/13 Receptor and Is Blocked by an Elevation of cAMP

In the previous study by Honda et al. (2001), extracellular ADP induced microglial chemotaxis through Gi-coupled P2Y receptors and the ADP-induced membrane ruffling was inhibited by a P2Y12- and P2Y13-selective antagonist, ARC-69931. First, to make the system closer to pathological conditions in the CNS, we performed the chemotaxis assay on fibronectin substrates. To examine whether microglial chemotaxis toward ADP on fibronectin substrate is also mediated by the P2Y12/13 receptor, ARC-69931 was used in the chemotaxis experiment (Fig. 1). Cultured microglia were adhered to the fibronectin-coated coverslips and their chemotaxis against the ADP concentration gradient was studied with the Dunn chemotaxis chamber (see materials and methods for details). In the absence of the ADP gradient, microglia did not move on the fibronectin-coated coverslips (Fig. 1b). When ADP 100 μM was applied to the system, however, the cells migrated toward the stimulant (Fig. 1a,c). Pretreatment of microglia with ARC-69931 at 10 μM totally blocked the ADP-induced microglial chemotaxis (Fig. 1d), suggesting that the P2Y12/13 receptor is responsible for the microglial chemotaxis toward ADP. Since the activation of P2Y12/13 receptors inhibits adenylate cyclase, the effect of changes in the intracellular cAMP level on microglial chemotaxis was tested. Forskolin is a potent adenylate cyclase activating agent and dibutyryl cAMP is a membrane permeable AMP analogue that activates cAMP protein kinases. When microglia were pretreated with forskolin (Fig. 1e) or dibutyryl cAMP (Fig. 1f), their chemotaxis toward ADP was greatly attenuated.

β1 Integrin Is Involved in the Microglial Migration Toward ADP on Fibronectin Substrate

To study the function of β1 integrin in the P2Y12/13-receptor mediated migration of microglia, we first examined its expression on cultured microglia. Flow cyto-

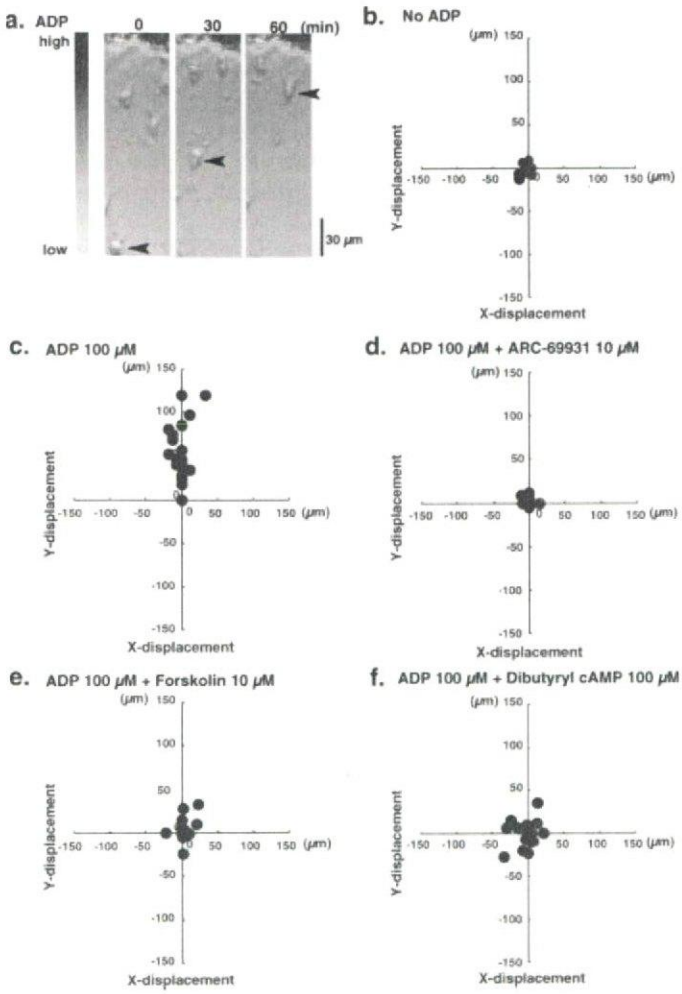

Fig. 1. ADP-induced chemotaxis of microglia was mediated through P2Y12/13 receptors and blocked by an elevation of intracellular cAMP. Cultured microglia were adhered to fibronectin-coated coverslips. After serum starvation, the cells were assayed for migration toward ADP in the Dunn chemotaxis chamber. **a:** Typical chemotactic responses of microglia toward ADP. Arrowheads depict the position of a single microglial cell at the indicated time, showing the kinetics of chemotaxis. Microglia were almost static on fibronectin in the absence of the stimulant (**b**). Microglia, however, showed chemotactic responsiveness to ADP (100 μM) (**c**), which was completely blocked by the P2Y12/13 receptor antagonist ARC-69931 (**d**), confirming that the chemotaxis to ADP is mediated by P2Y12/13 receptor. Forskolin pretreatment (**e**) and dibutyryl cAMP pretreatment (**f**) attenuated the ADP-induced chemotaxis of microglia. The data represent three independent experiments.

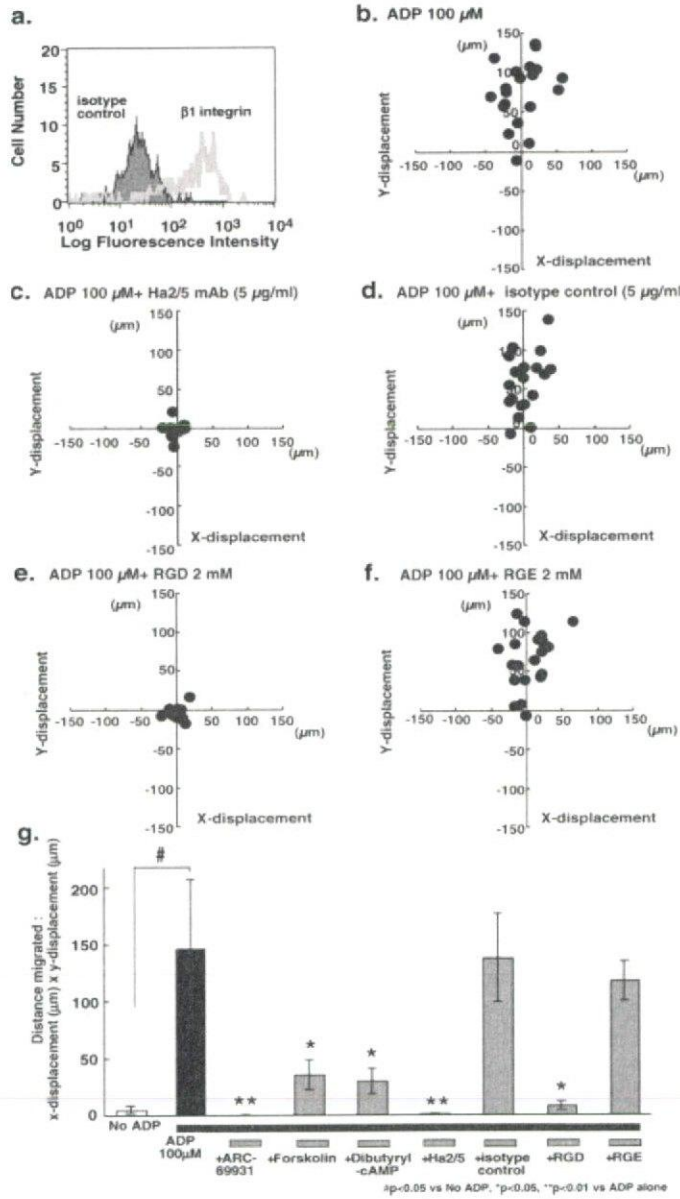

Fig. 2. β1 integrin is highly expressed on cultured microglia, and it is involved in the ADP-induced chemotaxis of microglia on the fibronectin substrate. Cultured microglia were labeled with anti-β1 integrin antibody (Ha2/5) (gray) or with isotype-matched control antibody (black). The labeling was detected by Alexa-Fluor 488-conjugated antibody and the cells were subjected to flow cytometry analysis (**a**). **b–f:** Cultured microglia were adhered to fibronectin-coated coverslips. After serum starvation, the cells were assayed for migration toward ADP in the Dunn chemotaxis chamber. The microglia migration toward ADP (100 μM) (b) was totally inhibited by Ha2/5 (c) and RGD peptide (e). In contrast, the migration was not affected by isotype-matched control (d) and RGE peptide (f). Data (a–f) represent three independent experiments. Each chemotaxis was quantified by calculating the x displacement (μm) multiplied by the y-displacement (μm) (**g**). Data (g) are mean ± SE of three separate experiments. #Greater than No ADP ($P < 0.05$, Student's t-test); *Smaller than ADP 100 μM ($P < 0.05$, Student's t-test); **Smaller than ADP 100 μM ($P < 0.01$, Student's t-test).

metric analysis confirmed that the cultured microglia expressed significant amounts of the β1 integrin subunit (Fig. 2a). Next, to assess the role of β1 integrin in the cell migration toward ADP, a chemotaxis assay was performed with the Dunn chemotaxis chamber in the presence of a monoclonal antibody specific for the β1 integrin subunit (Ha2/5) and RGD peptide (Fig. 2b–f). Treatment of microglia with Ha2/5 antibody at 5 μg/ml suppressed the ADP-induced chemotaxis (Fig. 2c), indicating that β1 integrin is required for this process. An isotype-matched control antibody did not interfere with the microglial chemotaxis toward ADP (Fig. 2d). Treatment with RGD peptide at 2 mM also perturbed the microglial migration toward ADP (Fig. 2e), whereas control RGE peptide did not inhibit the migration (Fig. 2f), suggesting that the RGD sequence is important. The RGD (Arg-Gly-Asp) sequence is present in several extra-